Development of Polydopamine-Coated Particles for the Delivery of Therapeutic Agents Post-Myocardial Infarction

A thesis submitted in partial fulfilment of the requirements for the degree of

Masters of Applied Science

Biomedical Engineering

by

RojaGauda

Department of Biomedical Engineering
Faculty of Engineering
University of Ottawa

Ottawa-Carleton Institute of Biomedical Engineering

DECLARATION

I hereby declare that the thesis entitled “Development of Polydopamine-Coated Particles for the Delivery of Therapeutic Agents Post-Myocardial Infarction” submitted by me, for the award of the degree of Master’s of Applied Science from the University of Ottawa, is a record of bonafide work carried out by me under the supervision of Dr. Erik Suuronen, PhD, Division of Cardiac Surgery, University of Ottawa Heart Institute and Dr. Fabio Variola, PhD, Faculty of Engineering, University of Ottawa. I further declare that the work reported in this thesis has not been submitted and will not be submitted, either in part or in full, for the award of any other degree or diploma in this Institute or any other Institute or University.

The entire study was designed and executed in its entirety with the efforts of Prof. Erik Suuronen, Prof. Fabio Variola and myself and I am the sole author of the relevant written work.

ABSTRACT

Successful delivery and maximal retention of therapeutic agents at the site of injury is important for cardiac repair post-myocardial infarction. Polydopamine (PDA) is considered a bioadhesive with excellent adhesion properties. This thesis aims to develop and test a PDA coating that can be applied to the surface of delivery particles so as to increase their adhesion strength and thus improve their retention at the site of infarction post-delivery. As a proof-of-principle, we investigated whether PDA coating on fluorescent beads confers a better retention rate at the site of delivery compared to non-coated beads. The first part of the study focused on the optimization of the PDA coating so as to finalize a deposition time for the coating process which will have the maximum adhesion strength. Once the PDA protocol with maximum adhesion strength was identified, PDA coating was performed on commercially available fluorescent beads. The viability of cultured macrophages and endothelial cells was not different when exposed to PDA-coated fluorescent beads compared to non-coated beads. *In vivo*, PDA-coated or non-coated beads were sprayed onto the surface of the mouse myocardium and their retention was evaluated at 3 hours and 1 day post-delivery. Fluorescence imaging results showed that the retention of PDA-coated beads on the myocardium was significantly greater than for non-coated beads at 1 day after application. These results suggest that PDA coating may be a strategy to improve the retention of carriers delivering therapeutic agents for the treatment of myocardial infarction, thus potentially improving therapeutic efficacy.

ACKNOWLEDGEMENT

With immense pleasure and deep sense of gratitude, I wish to express sincere thanks to my supervisors Dr. Erik Suuronen and Dr. Fabio Variola, without their motivation and guidance, this research would not have been a success. In addition, I would like to thank them for their faith and confidence in me, allowing the research freedom and funds to attempt experiments successfully.

I express my sincere thanks to my lab mates Cagla Cimenci, Hiroki Takaya, Marcello Munoz, Ines Amara, Xixi Guo, Irene Guzman, Alexander Steeves and Nidhi Agrawal for their help in my experiments, continued support, encouragement and shared love whenever I needed them the most.

I wish to extend my profound sense of gratitude to my parents Mrs. Reena Gauda and Mr. SurendraNath Gauda for providing me with not only the love, support and resources that allowed me to complete my research but also giving me the opportunity to come so far all the way from India to Canada to achieve my dreams and to always in believing that I was capable to do so.

To my sister Pooja Gauda, who always has my best interests in heart and has been a constant source of protection, love and reason at any time of the day, no matter what. Also love and thanks to all my family members for always believing in me and showing me their support at every aspect.

Last but not the least; I would like to thank my friends who have always been by my side in giving the best time throughout my highs and lows.

Table of Contents

LIST OF FIGURES

LIST OF TERMS AND ABBREVIATIONS

AC	Alternating Current
ACC	Animal Care Committee
AFM	Atomic Force Microscopy
ANOVA	Analysis of Variance
APS	Ammonium Persulfate
ATR	Attenuated Total Reflectance
CCD	Couple Charged Device
DHI	Dihydroxyindole
DI	Deionized Water
DOPA	Dopamine
DPFM	Digital Pulsed Force Method
EPR	Enhanced Permeability and Retention
FESEM	Field Emission Scanning Electron Microscope
FM-AFM	Frequency Modulation Atomic Force Microscope
FWHM	Full Width Half Maximum
HA	Hyaluronic Acid
HUVECS	Human Umbilical Vein Endothelial Cells
IHD	Ischemic Heart Disease
IVIS	In Vivo Imaging System
LV	Left Ventricle
MI	Myocardial Infarction

NC	Non-contact
NIR	Near Infrared Radiation
NOD-SCID	Non-Obese Diabetic Severely Combined Immunodeficient
PDA	Polydopamine
RFU	Relative Fluorescence Units
ROI	Region of Interest
SEM	Scanning Electron Microscope
SR	Sustained Release
UV	Ultraviolet

CHAPTER 1

Outline

1.1 Novelty and Contribution

The motivation of my proof-of-principle research was to obtain a PDA coating on nanoparticles as an approach to improving the adhesiveness and retention of therapeutic particles in the heart for the treatment of myocardial infarction (MI). To this end, my thesis was aimed at evaluating this strategy by using commercially available fluorescent beads in a mouse model of MI. The thesis was divided into two parts.

(1) The first part of the study was focused on optimization of the PDA deposition protocol. This was carried out by coating glass coverslips with PDA to evaluate the homogeneity and adhesive strength of the resulting coating to obtain the conditions which provide the highest adhesive strength. As per my results, the adhesion strength is not very much affected by the deposition parameter I investigated, namely the deposition time. However, it was observed that a gradual increase in deposition time might result in lower adhesion.

(2) In the second part, the PDA protocol was used to coat commercially available fluorescent beads to evaluate the coating effects on biocompatibility *in vitro* and bead retention *in vivo*. It was found that the coating did not affect the ability to detect the beads' fluorescence, nor did it affect cell viability when added to cultures of macrophages or endothelial cells. *In vivo* experiments revealed that there is a significant increase in the retention of PDA-coated beads when sprayed onto the surface of the myocardium of mice compared to non-coated beads.

1.2 Outline of Thesis

Chapter 2 provides a basic introduction of MI, fluorescent nanoparticles, polydopamine (PDA), atomic force microscopy and *in vivo* fluorescent imaging techniques.

Chapter 3 explains the materials and methods used in the study.

Chapter 4 discusses the results and analysis of the different experiments including the structural analysis which was carried out using Scanning Electron Microscopy and Atomic Force Microscopy, physiochemical analysis using fluorescence spectrometry to verify if PDA is masking the fluorescence of the beads, cell viability tests using macrophages and endothelial cells to check biocompatibility and finally In vivo Imaging System to evaluate the myocardial retention of coated and non-coated beads in a mouse model.

Chapter 5 discusses the conclusions derived from this study and how we can proceed in further studies using these results.

CHAPTER 2

Introduction

Myocardial infarction followed by a heart failure still continues to be one of the leading causes of death [1] and a promising direction for the delivery of therapeutic agents for treating this disease is the use of biomaterials. Nanoparticles are considered attractive for minimally invasive delivery of therapeutic agents due to their small size and the ability to administer them via multiple injection methods [2]. In order to aim for maximum retention at the infarction site, the use of biomaterials with great adhesive properties is important.

Another consideration in developing adhesive biomaterials for coating fluorescent nanoparticles is the inclusion of a fluorescence marker or other tracer that confers the ability to track the nanoparticles inside the body once they are injected. This strategy allows for the assessment of nanoparticle retention at the infarct region and to evaluate if maximum retention correlates with greater delivery of therapeutic agents and improved functional outcomes.

2.1 Myocardial Infarction

Myocardial infarction (MI), also commonly known as a heart attack, in simple words can be defined as myocardial cell death. As per a report in 2017 by the Global burden of disease study, cardiovascular diseases have been the main cause of death around the world [3-4]. Almost half of all the cardiovascular deaths are caused by ischemic heart diseases (IHD) [4], and MI is the main cause of death among all the IHD.

2.1.1 Fundamental Concepts of Myocardial Infarction

MI is mostly caused by a decrease in the supply of blood flow to a portion of the heart thus leading to necrosis of that portion of the heart muscle [5]. In every living tissue, including heart muscle, the oxygen demand should be equal to the blood supply which is

known as supply-demand ratio and when this balance is disturbed, it causes damage to that particular tissue. In the case of heart muscle, this imbalance may be caused due to a very rapid heart rate resulting in increased oxygen demand or due to a drop in blood pressure resulting in too little supply of blood and this may lead to myocardial damage and thus MI [5]. MI is becoming increasingly common in developing countries with more than 3 million people suffering acute ST-elevated MI and over 4 million people with non ST-elevated MI per year, thus making it a major cause of mortality and morbidity worldwide [6]. The occurrence of MI can be considered as the first manifestation of coronary artery disease [7]. MI often results from the rupture of a vulnerable plaque in a coronary artery causing a thrombotic occlusion [8], which leads to ischemia due to imbalance in the supply-demand ratio of the myocardial muscle. And this myocardial cell death caused due to prolonged ischemia can lead to massive myocardial cell death (MI). After the onset of myocardial ischemia, cell death takes a finite period of time to develop. MI can be classified based on the size - microscopic (focal necrosis), small (10% of the left ventricular [LV] myocardium), moderate (10 – 30% of the LV myocardium) and large (>30% of the LV myocardium) [7]. MI leads to a massive sudden loss of cardiomyocytes. In order to treat MI, many therapies have been used; among them thrombolytic therapies are commonly used which result in myocardial reperfusion. However, it has been found that even after restoration of blood flow, there still occurs cardiomyocyte death [9], which leads to ischemia reperfusion injury [10] as well as increases in ventricular loading and excessive physical forces [11]. This leads to programmed cell death in myocardium. The sudden loss of this large amount of cardiomyocytes at the infarct region [12] leads to lowering of the ejection fraction (**Figure 1**). The region of the left ventricle which was supplied by the obstructed coronary artery [13] as well as the surrounding surviving region of the adjacent wall as well as the region remote to the infarcted region undergo programmed cell death of myocytes [14]. The heart has a very limited ability for regeneration and so that the cardiomyocytes that die post-MI are lost permanently.

2.1.2 Repair after Myocardial Infarction

A healthy heart consists of a lot of different types of cells that function together in order to maintain the optimal function of the heart [15]. However, in the diseased heart there is

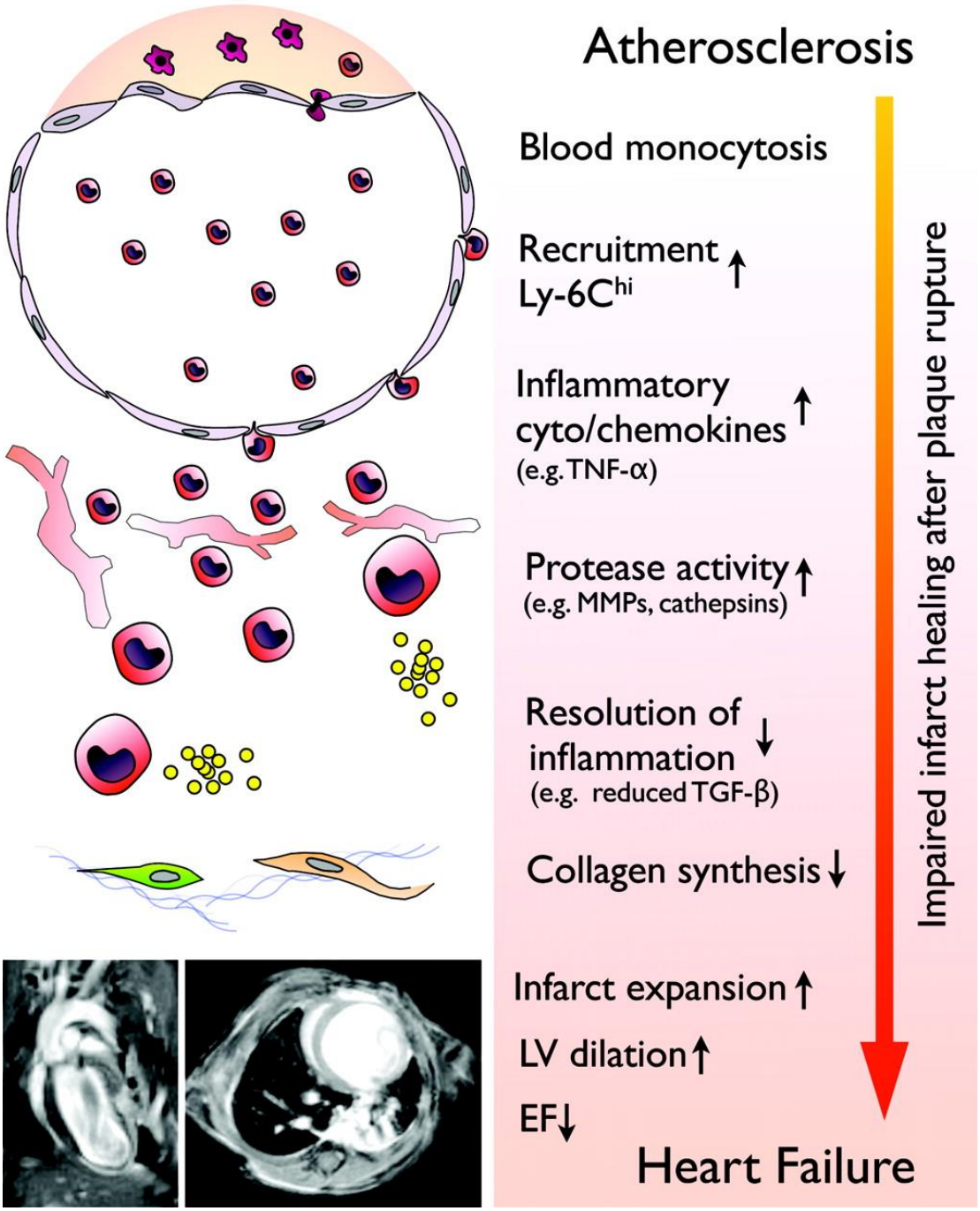

Figure 1. Atherosclerosis leading to heart failure

Following MI there is an increased number of inflammatory monocytes at the infarct site. Increased recruitment of monocytes leads to impaired healing and ultimately the development of heart failure if ventricular remodelling occurs and loss of cardiac function cannot be minimized. Reproduced from [16] with permission.

an impact on one or more cell types, which in turn reduces normal heart function. Following MI, the heart undergoes healing that involves 3 overlapping phases: the inflammatory phase, the proliferation phase and the maturation phase (**Figure 2**). In the inflammatory phase, the initial massive loss of cardiomyocytes post-MI leads to the activation of inflammatory signals that result in the recruitment of macrophages in order to clear the debris [15]. In the proliferation phase, there is a continuous recruitment of leukocytes and secretion of matrix protease thus leading to scar formation due to the invasion of fibroblasts and due to the irreversible loss of myocardial cells [17]. The fibroblasts release large amounts of extracellular matrix proteins like collagen at the infarct size which forms the collagenous scar in order to prevent the heart tissues from any kind of ventricular rupture [18]. However, the scar that forms is very rigid, and it does not synchronize with the beating of the heart. This in turn can lead to formation of cardiac-dilation, hypertrophy and cardiac failure [19-23]. Therefore, therapies are needed that can replace the lost cardiomyocytes or that can limit the extent of damage and prevent heart failure post-MI. Such therapies should be implemented within 1 to 2 weeks of the onset of MI since beyond this period shows extensive changes in the tissue architecture and the heart undergoes significant changes in the ventricular function and its geometry [16]. If functional preservation or restoration is not achieved in this period, it may lead to expansion of the infarct size and left ventricular dilatation (ventricular remodelling), loss of contractile capacity (heart failure) and ultimately rupture of the scar and death and in long [24-26]. So, it is important to augment the wound healing process soon after MI. Due to the limited regenerative capacity of cardiac cells, various technologies have been developed and tested to achieve this. One such approach is biomaterial therapy, which has been able to promote the restoration at the infarct region by improving the survival and function of the different types of cells involved in repair and regeneration. Biomaterials may also be used for the delivery of external therapeutic agents that promote repair and the restoration of heart function. The application of these therapeutic agents would benefit from delivery systems that can improve their retention specifically at the infarct region.

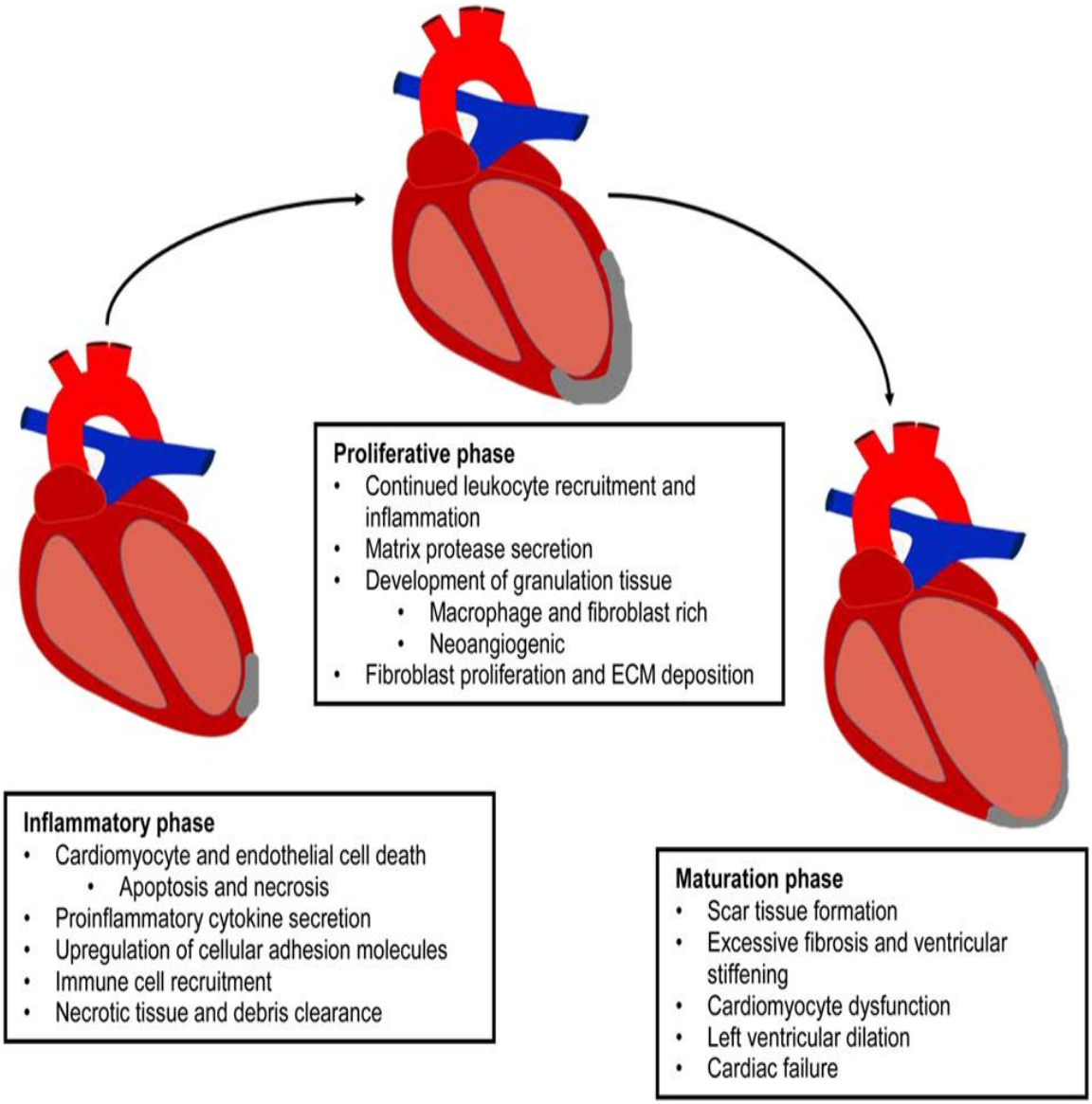

Figure 2. Evolution of the infarcted myocardium

MI results in activation of a multiphase healing process consisting of three phases namely the inflammatory phase, proliferation phase and maturation phase. This is a natural healing process which takes place to prevent ventricular rupture; however, it is not sufficient to protect the heart from huge tissue loss and can lead to heart failure. Reproduced from [15] with permission.

2.2 Nanoparticles as Delivery Agents

Barriers to the delivery of therapeutics to the infarcted heart include the immune response, the physical cellular barrier, the mechanical force of blood flow, anatomical challenges of access and also low survival rate (for cell therapies) in the harmful microenvironment of the host cardiac tissues where the treatment is delivered. There are many drugs for treating MI that might have poor solubility in blood and/or have a short half-life in the circulation, and this leads to reduced accumulation of these compounds at the infarct region [27-29]. Other therapies such as cells, small molecules and growth factors that are applied directly to the myocardium also suffer from low retention and thus reduced therapeutic effects. When therapeutic agents are directly injected into tissue, there is a chance that they might not be retained at that particular site due to environmental factors that limit retention or physical forces (such as a beating heart) that cause extrusion of the therapeutics. Therefore, more efficient delivery systems are needed to improve the therapeutic efficacy of such treatments. To this end, injectable biomaterials, microparticles and nanoparticles are being tested as vehicles that can be loaded with these agents like cells, small molecules or growth factors to enhance their delivery at the target site [30-31]. Nanoparticles have been proven to be one of the most efficient injectable biomaterials for the delivery of therapeutics. In order to achieve these therapeutic effects it is important to achieve target-specific delivery of these agents [22]. In one strategy, enclosing agents inside nanoparticle-sized carriers can prevent the agents from diffusing to the neighbouring areas by modification of the surface of the nanoparticles with different target groups which make it possible for them to bind to specific groups at the target site and thus make target specific delivery and release of the therapeutic agents. After the onset of MI, there is occurrence of cardiomyocyte death and negative remodelling of the left ventricle makes it important that the therapeutic agents enclosed in biomaterials are delivered in a minimally invasive way. Hence, nanoparticles due to the Enhanced Permeability and Retention (EPR) effect, are well-suited for this purpose [2]. Apart from this, nanoparticles also have a high payload compared to macro-sized particles, which makes them a better choice as delivery agents. There have been a number of studies where micro- and nanoparticles have been used as carriers to deliver therapeutic agents for treating ischemic tissue. In one such previous study, where vascular endothelial growth factor (VEGF) was loaded into poly lactic-co-glyocolic acid

(PLGA) nanoparticles and then delivered intravenously into a mouse femoral artery ischemic model, and its efficacy was compared to VEGF delivered without the use of nanoparticles. The results showed a significant increase inconnectivity as well as increase in the total vessel density in the mice treated with VEGF-loaded nanoparticles. The results also indicated an improved anastomosis at the vascular bed demonstrating that VEGF loaded into PLGA nanoparticles have an improved specificity leading to better therapeutic effects [23]. In another study, loading adipose-derived stem cells into polymeric microparticles prolonged their survival upon delivery to the infarcted heart resulting in a superior therapeutic effect for up to 3 months post-transplantation compared to cell treatment alone [24]. In another work, PLGA nanoparticles were loaded with irbesartan and delivered at the infarct site after an ischemia/reperfusion injury; results showed a 17-fold increase in irbesartan concentration compared to delivery of the free drug, resulting in enhanced tissue recovery [25]. All these studies have shown how encapsulation within particles can improve the efficacy of therapeutics due to their ability to control the release of the loaded agents and to remain in the circulation/tissue for a greater period of time. Despite the promise of micro- and nanoparticles for the delivery of therapeutics for treating MI, optimal retention and therapeutic potential has not yet been achieved due to the barriers described above.

2.2.1 Fluorescent Nanoparticles

An attractive feature of nanoparticles is that they allow for the use of optical imaging techniques through the incorporation of tracking compounds such as fluorescence or magnetic elements. This confers easy detection for their study in vivo, such as for visualizing vascular permeability, tracking and evaluating the delivery of their cargo and their presence at the target site and also tracking uptake by different cell types [22]. Our study focuses on the retention of the nanoparticles at the target site and will be using the optical imaging techniques for the detection process. Even though in vivo optical imaging techniques have some limitations including the issue of limited tissue depth penetration in whole animals due to thick and opaque tissues, these issues have been somewhat overcome with the use of Near Infrared Radiation (NIR) probes allowing the better detection of fluorescence.

2.3 Polydopamine

The effective delivery of therapeutic agents at the infarct site requires maximum retention of the delivery vehicle at that site and this can be achieved by functionalizing the surface of nanoparticles with an adhesive material. PDA, a biopolymer material inspired by the adhesive nature of amines and catechols found in adhesive proteins in mussels, has excellent adhesiveness and cell affinity [26]. Coating the nanoparticles with PDA is expected to result in improved adhesion when applied to wet tissue surfaces and thus result in better retention at the infarct site.

2.3.1 Structure

The proteins found in mussels, namely the *mytilus* foot proteins-3 and -5 (Mfp-3 and -5), that are located in the distal portion of the mussel byssus where the byssal foot engages the surface of the substrates have two main features that inspired the development of PDA [27-28] (**Figure 3**). These two features include: (1) high catechol content (3,4-dihydroxybenzene) due to the presence of DOPA (3,4-dihydroxy-L- phenylalanine); and (2) high content of primary and secondary amines contributed by the lysine and histidine residues [29]. The development of PDA mainly involves the oxidation of dopamine at an alkaline pH. The oxidation product of this reaction is dopamine quinone which then goes through a nucleophilic intramolecular cyclization process in order to form 5,6-dihydroxyindole (DHI) and these two compounds, dopamine-quinone and DHI together, lead to the formation of PDA [29].

2.3.2 Adhesive Strength

With most of the conventional adhesives that are currently available when used with wet substrates, the interfacial water molecules create a barrier to the adhesives by blocking the interactions between the substrate and the adhesive thus leading to a failure to adhere [38-39]. In contrast, PDA contains catechols, phenyl and amine groups, and the presence of these groups contributes to its great adhesive strength. The interaction of these groups with various substrates using hydrophobic, electrostatic and hydrogen bond interactions [31] can occur not just in normal conditions but also under aqueous conditions [32], making PDA an attractive option for use as a biological adhesive. The mussel foot consists of around 15 such proteins, of which Mfp-3 and Mfp-5 consist of 20-30 mol % of Dopa, Lys and Arg present at the adjacent positions in the protein

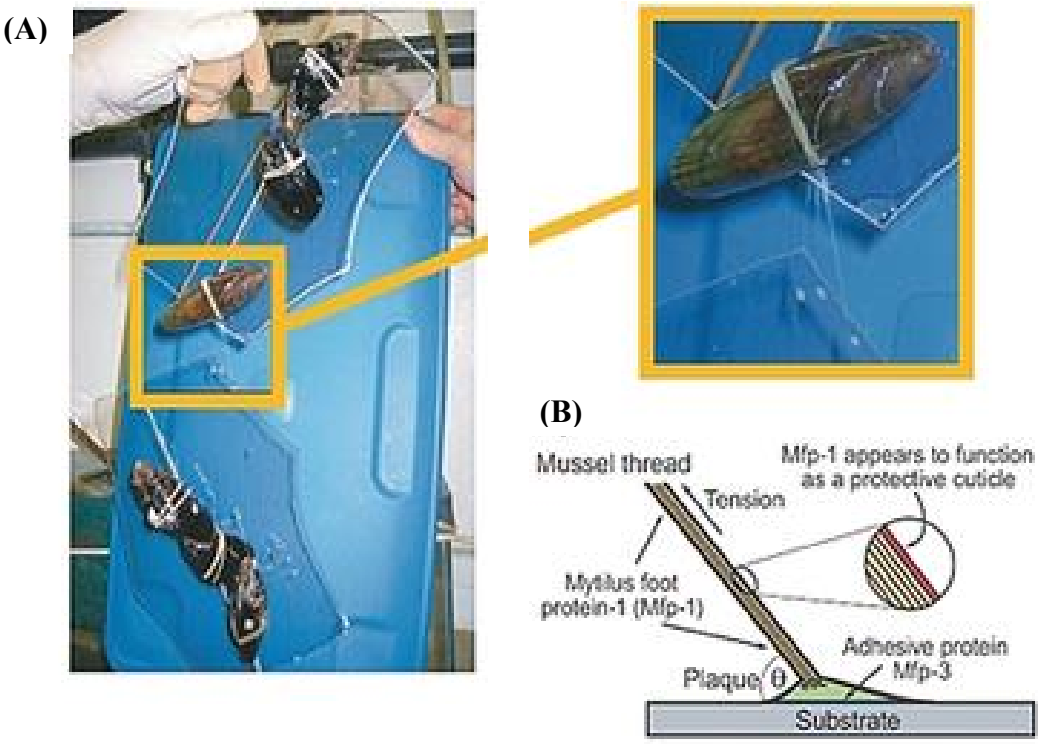

Figure 3. Adhesion Proteins of Mussels

(A) Image showing mussels adhered to mica surface and the enlarged image. (B) Schematic representation to show byssal thread attachment to substrate. Reproduced from [33] with permission. Copyright:© 2019 Wiley-VCH Verlag GmbH & Co. KGaA, Weinheim

backbone [30]. The combined effects of both the DOPA and lysine in mussel foot proteins tend to have low interfacial energy [34] thus making them adhere strongly underwater; PDA is designed to have a similar structure and can thus adhere to almost all surfaces [35].

2.3.3 Deposition

Various factors such as pH, buffer solution, solvents, temperature and reactant concentrations lead to variations in the formation of PDA, be it the film thickness of PDA surface coating or the size of the formed PDA nanoparticles [44-47]. PDA can be used to produce catecholamine-based coatings in the presence of Tris buffer at a pH of 8.5 along with naturally dissolved O_2 in the water as an oxidant [37]. Other than the dissolved O_2,other oxidants such as ammonium peroxodisulfate and sodium periodate [38], or UV irradiation [39] may be used in order to generate free oxygen species thus helping in the polymerization process of dopamine leading to formation of PDA. One of the major advantages of using light for the deposition process is that it helps to control the onset and the termination of the PDA coatings and also controlling the amount of light can be useful in creating desired patterns of the PDA coating on the substrate surface [29]. Another method for forming PDA coatings is electropolymerization in an electrolyte dependent manner [40]. However, in this case the film thickness reaches a maximum constant after which the dopamine present in the solution can no longer be oxidized [41] and this leads to the presence of unoxidized dopamine particles, thus resulting in their deposition and formation of aggregates on the substrate surface. In addition to the reaction conditions, the process used for coating also has an impact on the features of coated films. Dip coating is the traditional method wherein the substrate is simply dipped inside the prepared polymer solution for the desired amount of time. A number of other different ways of coating PDA on surfaces have been developed. PDA can be deposited using a spray-deposition method where a freshly prepared polymer solution under set reaction conditions is added to a gas-driven thin layer chromatography spray coater and then sprayed over the desired substrate surface until the surface is completely wet with the polymer [42]. Spray coating is considered to be better than the conventional dip coating method as the spray coating does not require any special vessel for the coating process and is thus suitable for coating of substrates which have a larger surface area. The spray coating is thus preferred when there is a need of coating

substrates in large scale industries. In the case of the Langmuir-Schaeffer method, PDA films are deposited at a water-air interface and then transferred to solid substrates [43]. The deposition rate is found to be impacted by the concentration of dopamine used; however the dopamine concentration usually cannot be increased much as this leads to the presence of excess dopamine particles [44] and formation of aggregates, which is believed to produce a non-homogenous coating and lower adhesive force. Another factor that might affect the deposition of PDA is the addition of motion to the coating process. In the static method of coating, which is the classic way of PDA deposition [45], the substrate is just dipped in the polymer solution without any added motion. One way of adding motion to the procedure is stirring, which is usually applied to limit particle deposition on the substrate, and another is shaking [59-60], where the dopamine solution is shaken in order to achieve a uniform PDA film on the substrate surface at different reaction temperatures and deposition times [61-63]. So, the deposition of PDA depends on a number of reaction conditions, as well as the type of PDA coating and/or type of PDA particles.

These deciding factors can be altered accordingly in order to get the desired final structure and coating. However, it is also important to consider the potential negative effects that these factors may have, such as aggregate formation with greater deposition times. Aggregate formation may be overcome by adding certain molecules that will be able to break these aggregates, thus it becomes important to carefully optimize the deposition process. Previous studies looking at the stability of PDA films deposited on a silicon substrate showed that the films were stable for a minimum of 4 days in the presence of physiological buffer solution [41].

2.4 Atomic Force Microscopy

Atomic Force Microscope (AFM) is one of the most versatile and unique types of scanning probe microscopes, which works on the concept of using force to image a surface. The forces that are used may be magnetic, electrostatic, van der Waals, capillary [48] or interatomic forces between the tip used to probe the surface and the surface to be imaged. The main components include a probing tip on a cantilever spring, a method to detect the deflection of the cantilever when it moves on the surface, a feedback system which is used to control the deflection of the tip, a scanning system and a display system

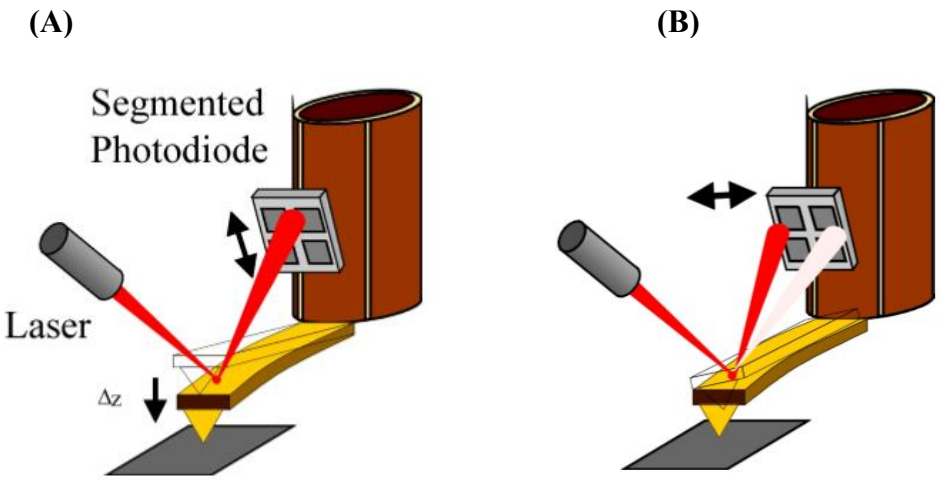

Figure 4. AFM setup and Force Distance Curve

(A) A typical AFM setup. (B) AFM setup in case of friction measurements. Reproduced from [49] with permission.

(**Figure 4A**)[50]. AFM is used to image minute topographic features on a surface along with probing other surface properties including adhesion forces, magnetic and conductive properties, out of which its use in adhesion force calculation will be exploited in our study. AFM usually consists of two major modes, the amplitude modulation atomic force microscopy (AM-AFM) and the frequency modulation atomic force microscopy (FM-AFM) [51]. The WITec Alpha300 RSA model of the AFM used in our lab works in three modes, namely the contact mode, non-contact mode and digital pulsed force mode (DPFM).In the contact mode, the tip is in contact with the surface throughout the imaging process and the spring constant of the cantilever plays the most important role in determining the forces between the tip and surface to be imaged. Non-contact (NC) mode is a type of AC mode of AFM where in the tip experiences very little interaction with the surface and a very small amount of force is applied between the tip and the surface thus allowing for a better resolution of the image formed. In the DPFM, AFM operates in a contact mode but in a sinusoidal way and it takes a force-distance curve at every point of the image [52].

2.4.1 Contact Mode Analysis

As mentioned previously, the contact mode puts the tip in continuous contact with the surface. Bending of the cantilever is considered as the feedback parameter in this case. The scan stage where the surface to be imaged is kept experiences an up and down motion that helps image the surface topography. Depending on the surface topography, the cantilever tips will bend and this deflection of the tip is recorded by the detector which is then converted into the image. The data acquired in AFM contact mode analysis is presented in three ways:1) the line scan, where force distance curves are measured over a line on the surface, 2) the image scan, where the entire contact mode image is taken, and 3) the distance curve, where the force distance is measured at the current position. In contact mode AFM analysis, there is an application of lateral forces (**Figure 4B**) as well as the common vertical forces between the cantilever tip. The presence of lateral forces may result in the removal of some of the loosely bound particles on the surface of the substrate and this might lead to a lower resolution of the image, which is why it is recommended to use those cantilever tips that exert less force between the tip and the surface thus tips with spring constant less than 1N/m should be used to get good resolution images.

2.4.2 Force-Distance Curve

The force-distance curve for a point is plotted using the tip approach and retract method which are mostly used in the study of different surface properties like adhesion, elasticity, Hamaker constant, and hardness [53]. It is basically the plot of the tip sample interaction force against the tip sample distance [54]. When the force-distance curves are measured, the cantilever probe is moved in a direction perpendicular to that of the surface instead of the horizontal direction along the surface. The tip is slowly approached toward the sample surface and there is an attractive force between them until it comes very close to the sample and repulsive forces start. These repulsive forces bend the cantilever. However, a force is applied by the cantilever on the surface so as to keep the cantilever bending at a constant value. When the tip approaches the sample, the main force acting between them is the van der Waals force and if we consider the tip sample distance to be z, then the van der Waals force can be represented as the following:

$$V_{sample}(z) = Az^{-12} - Bz^{-6} \quad (1)$$

where A and B are the interaction parameters. The cantilever where the tip is attached is either of the rectangular or V shaped and has a spring constant value of k, is subject to a force which can be represented as

$$V_{cantilever}(z) = k(z-z_0)^2 / 2 \quad (2)$$

where z_0 is the tip sample distance when the cantilever experiences no bending at all. The combined resulting force of the van der Waals force and the elastic force is plotted along the distance value thus giving a force distance plot as shown in **Figure 5**. These force distance curves can be used to measure different properties including adhesion force which were used in our optimization step for PDA coating.

2.4.3 Adhesive Force Assessment

The adhesion force is basically the pull-off force that is required to pull the tip off of the sample surface. When the tip is in contact with the sample surface, it experiences an attractive interaction and the force that will be required to overcome these interaction forces to move the tip away from the surface will give us how strongly the surface was adhered to the tip, thus giving us a value for the adhesion strength of the surface. This

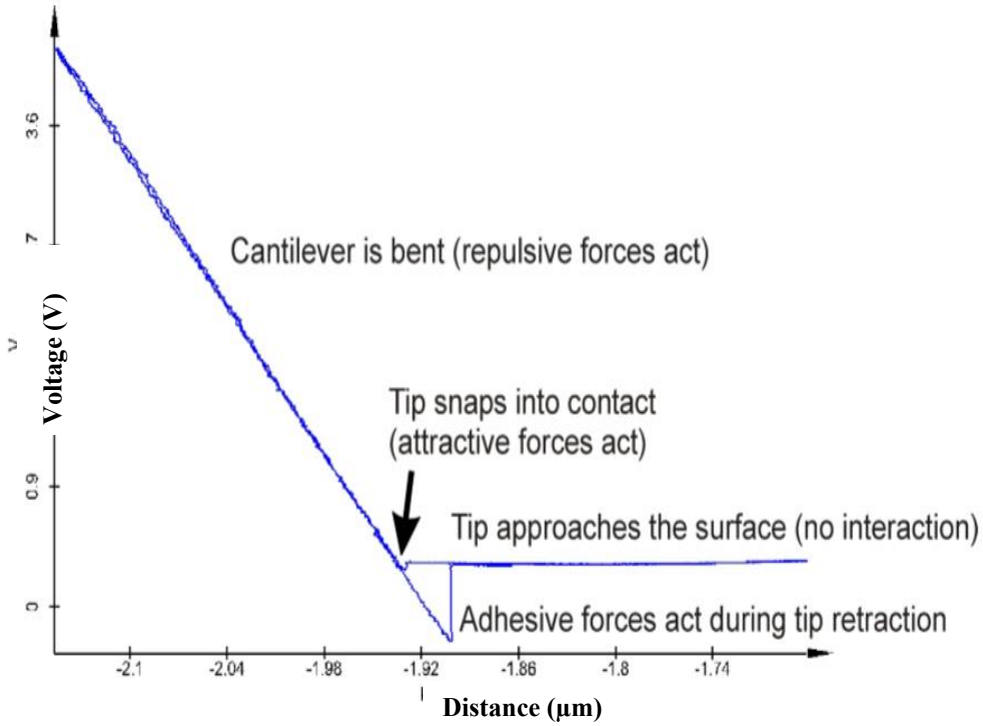

Figure 5. Force Distance Curve

Typical Force Distance Curve showing approach and retraction of tip and surface. Reproduced from [49] with permission.

adhesion force is equal to the jump off deflection of the cantilever multiplied by the spring constant of cantilever. The AFM readings give the voltage values from which the force values need to be derived and plotted against the distance. The relationship between the force and voltage values can be represented as:

$$\boldsymbol{Force(z) = Voltage(z) * Sensitivity * k} \quad (3)$$

where the sensitivity and k are obtained using the Sader method [55] while calibrating the tip.

The force values obtained are then plotted against the distance to get the force-distance curve. Adhesion force is then calculated from the force-distance curve as:

$$\boldsymbol{F_{AD} = |Minimum\ value\ on\ the\ curve - Baseline\ Value|} \quad (4)$$

The difference between the minimum value on the curve and the baseline value gives the adhesive strength of the substrate surface. This assessment can be done over the entire surface using multiple line scans over the area and averaging them out and the average work can be found out by calculating the area of the adhesion part in the force-distance curve.

2.5 In vivo Fluorescence Imaging

Our study uses fluorescence imaging to detect fluorescent beads in the extracted hearts of mice *ex vivo*. The in vivo imaging system (IVIS) uses a very sensitive camera in order to detect the fluorescence emitted from fluorescence emitting molecules in the whole living animal or from the extracted whole organs instead of cells on culture dishes [56]. So, IVIS provides both molecular imaging, where biomarkers are used for visualizing cell functions and anatomical or morphological imaging, where intrinsic properties of tissues are used for their visualization [57]. In vivo fluorescence imaging can be utilized for the detection of either autofluorescence of the living tissues or by using externally injected fluorophores. While imaging whole animals or living tissues in organs, thicker and opaque tissues will be able to absorb and/or scatter the light thus leading to lower signal intensity. Hence it can be beneficial to use fluorescent probes that emit in the near infrared region (NIR) (**Figure 6**) and while using external fluorophores, it is important to eliminate the autofluorescence caused by the surrounding living tissues and amplify the

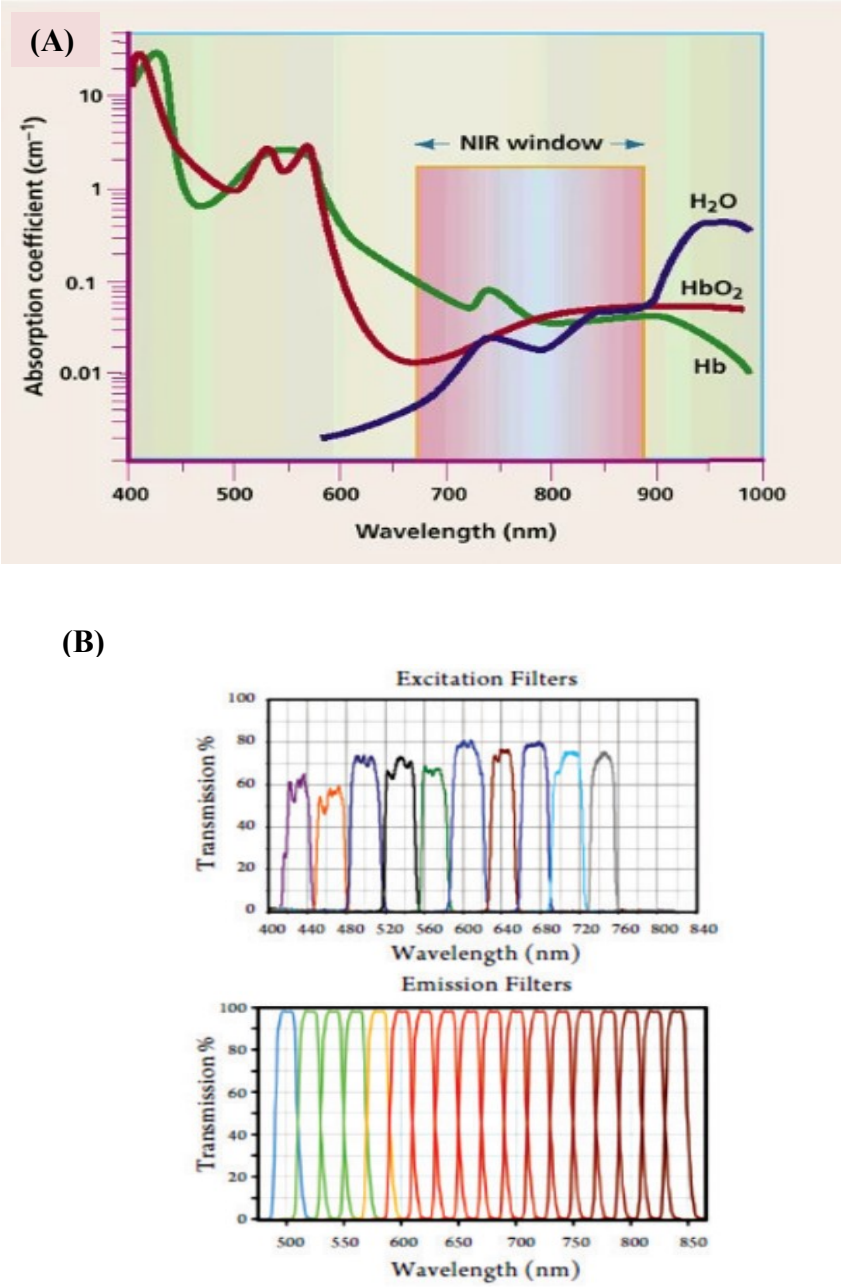

Figure 6. Fluorescence window for IVIS imaging

(A) NIR window works best for IVIS imaging as there is minimum light absorption by haemoglobin (<650 nm) and water (>900 nm) [58]. (B) Excitation and emission filters. Reproduced from [59] with permission. Copyright 1998-2016 PerkinElmer, Inc., U.S.A.; all rights reserved.

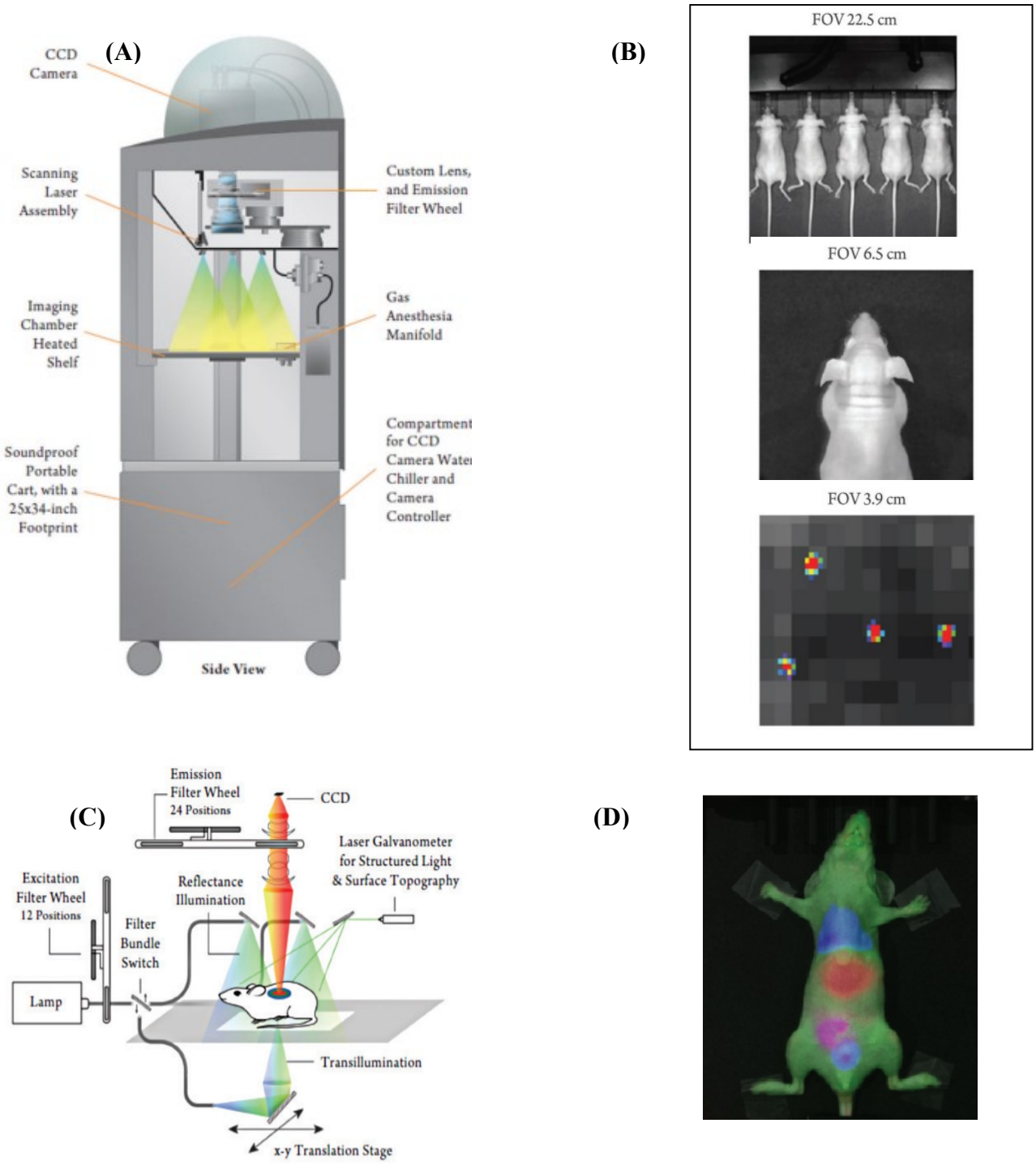

Figure 7. Components and use of PerkinElmer IVIS Spectrum

(A) Major components of IVIS Spectrum. (B) Basic working of IVIS imaging. (C) Different field of views starting from visualizing whole animals to single cells. (D) Spectral unmixing allowing detection of four different reporters. Reproduced from [59] with permission. Copyright 1998-2016 PerkinElmer, Inc., U.S.A.; all rights reserved.

desired signals [60]. For example, it might happen that fluorophores are injected to bind specifically to certain target sites for diagnosis, but autofluorescence signals are also emitted from the surrounding tissues that interfere with the fluorescence of interest in the target region. Using NIR fluorophores however, can help reduce the autofluorescence significantly. *In vivo* imaging of tissues has been increasingly used in fields such as oncology for the early diagnosis of malignant lesions and to study the tumour size and its spread to the adjacent tissues, cardiovascular diagnosis to identify the position of infarct region or for the detection of used treatment to verify its effectiveness and for other tissue metabolic studies [61]. The main reason behind the popularity of in vivo imaging system has been that it allows for imaging in native and real time physiological state, provides spatial location of the target site allowing its visualization with respect to time, and comes with the ability to repeat the experiments on the same specimen; Thus, it has become an important tool in the translation of clinical applications [62].

The IVIS system in our Institute is the PerkinElmer IVIS Spectrum which uses 3D diffuse fluorescence tomography, and has the ability of scanning 5 mice at a time (**Figure 7A-B)**. It allows for either trans-illumination, which occurs from the bottom and is used for illuminating the internally present fluorophores in imaging whole animals, or epi-illumination which occurs from the top and is used for surface illumination for imaging organs having fluorophores on the surface. Trans-illumination is a good choice for specific detection of more deeply located target sites and it also reduces the occurrence of autofluorescence of tissues. It allows the use of both fluorescent and bioluminescent reporters. The main components of IVIS Spectrum include an imaging chamber, CCD camera and custom lens, emission filter wheel and gas anesthesia manifold (**Figure 7C**). It allows spectral unmixing which makes it possible for the detection of fluorophores in different emission range and also helps reduce the effects of autofluorescence of tissues by separating them from different external reporters (**Figure 7D**).

CHAPTER 3

Materials and Methods

3.1 Preamble

This section contains all the materials and methods used in the entire study starting from optimization of the PDA coating material, to the *in vitro* experiments for PDA coated fluorescent beads, to the animal testing of the coated fluorescent beads. Shared information is included in the section with study specific information.

3.2 PDA Optimization on Glass Coverslip

Before coating the PDA on the fluorescent beads, the PDA coating was optimized on glass coverslips to obtain a protocol that will result in a homogenous coating with the maximum adhesive strength. The optimization steps were carried out considering different parameters that might affect the adhesive strength of the PDA coating. A 10 cm culture plate was taken and parafilm was added to fully cover the base of the culture plate. Once the parafilm was fully applied on the culture plate, coverslips were put on the culture plate and pushed so that they stuck firmly to the parafilm to make sure they do not move from their place while shaking. Once the coverslips were in their place, 25 mg of dopamine hydrochloride was added into 50 ml of solvent (Tris HCl or NaOH or Ethanol) depending on the specific protocol investigated to get a PDA concentration of 0.5 mg/ml. Similarly, the other concentrations of PDA were prepared. Once dopamine hydrochloride was added, the falcon tube was gently shaken to get the final sample. Once it was done, 30 ml of the sample was poured onto coverslips in the culture plate and was kept for shaking for the desired shaking time. Three coverslips per condition were coated. Once the deposition was done, the contents were aspirated and the coverslips were rinsed once with DI water and left for drying (**Figure 8A**). Once the coverslips were dried they were put in a 24 well plate and sealed with parafilm and tin foil. For all the experiments, clean coverslips were used. To get clean coverslips, they were placed one at a time in a

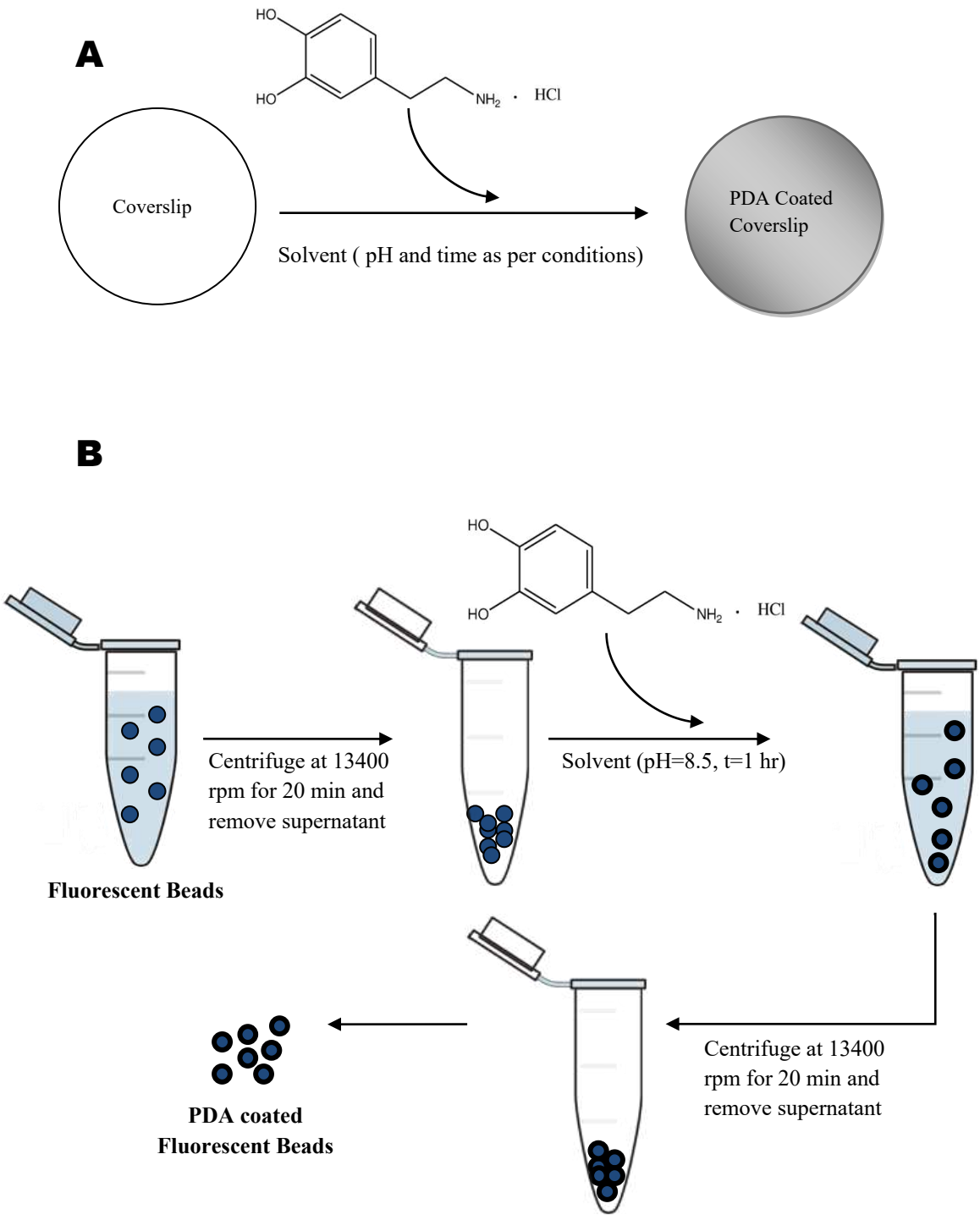

Figure 8. Schematic figure showing sample preparation of PDA coating on coverslip and beads at set protocol.

Schematics of sample preparation **(A)** Coating of coverslips using polydopamine hydrochloride along with solvent at desired conditions **(B)** Coating of Polystyrene beads with PDA hydrochloride along with solvent at pH = 8.5 and deposition time of 1 hr.

500 ml glass beaker filled halfway with hot tap water and 5 ml of Hellmanex. It was made sure that the coverslips were separated from each other so that they do not stick together. They were then sonicated for 30 minutes in a water bath sonicator. The hot water was then taken out and the coverslips were rinsed 4 to 5 times by swirling with DI water and were then sonicated again in double distilled water for 30 minutes. They were then rinsed 3 times by swirling with 70% ethanol and again sonicated with 70% ethanol for 30 minutes. Finally, they were rinsed with autoclaved water by swirling and transferred to a cell culture dish with autoclaved water for storage.

3.2.1 Polymerization of Dopamine Hydrochloride using Different Solvents

Initially, PDA hydrochloride polymerization was tested using 8 different solvents: Tris Buffer 5mM, Tris Buffer 10mM, Tris Buffer 15mM, NaOH 5mM, NaOH 10mM, NaOH 15mM, 30% Ethanol (EtOH) and 70% EtOH. A fixed value of pH of 8.5 was taken for the 3 solvents. 0.5 mg/ml of PDA was obtained by adding 25 mg of dopamine hydrochloride to 50ml of solvent along with APS and left for shaking with a deposition time of 1 hour.

3.2.2 PDA Coating using Different Values of pH

After analysing SEM images of the above coated samples to check homogeneity, three of these solvents were selected for pH testing experiments. Dopamine hydrochloride was polymerized using Tris Buffer 5mM, Tris Buffer 10mM and 30% EtOH to get a PDA concentration of 0.5 mg/mL Buffer with a deposition time of 1 hour. However, this time three different pH values of 5, 7 and 8.5 were tested to determine the final sample which was then coated on samples.

3.2.3 Polymerization with Different Deposition Time

Based on the homogeneity of the coatings, a pH of 7 and 8 were selected and then the deposition times were varied for 1 hour and 3 hours and PDA coating was carried out using Tris Buffer 5mM, Tris Buffer 10mM and 30% EtOH.

3.2.4 PDA Coating for Different Concentrations of Dopamine Hydrochloride

Finally, the concentration of dopamine hydrochloride was varied from 0.5mg/ml to 1mg/ml. A concentration of more than 1 mg/ml was not considered, as previous studies

demonstrated that this concentration range would lead to aggregation of PDA and thus result in a non-homogenous coating [63].

3.3 Scanning Electron Microscope (SEM)

SEM imaging was accomplished with a JSM-7500F Field Emission Scanning Electron Microscope (FESEM, JOEL, Japan). The primary purpose was to ensure the effective coating of PDA on glass coverslips and test their adhesive strength after deposition on spherical particles. It was used to ensure a homogenous coating and to finalize a PDA coating which could be coated on nanoparticles.

3.4 Atomic Force Microscopy (AFM)

Imaging of control and PDA-coated glass coverslips was carried out with the AFM module of alpha300 RSA (WITec, Germany) system. Images were taken in contact mode and using cantilever FMV-A to get adhesion strength values for the non-coated and coated coverslips. Throughout the AFM experiments, 2 FMV-A tips have been used. The cantilever tip was calibrated resulting in a spring constant of 1.63 N/m and sensitivity of 105 nm/V for the first tip and a spring constant of 1.55 N/m and sensitivity of 119 nm/V for the second tip. The tip was changed in between in order to avoid any sort of discrepancies in the AFM reading due to the presence of contamination due to excessive use of one tip. In our study, we have exploited the AFM contact mode analysis using line scan along four different lines over the surface. The measurements were set such that force distance curves were measured at 5 points on the line and the 4 different lines should be such taken that they are in four different regions of the surface, giving an average value of the adhesion force calculated over the entire surface area. Images were taken for 3 samples per deposition condition, so, in all, an average of 20 force-distance curves was taken per sample to get the final adhesion strength, and for every iteration there were 3 samples per methodology thus making it to 60 force-distance curves per condition in one iteration. In total an average of 180 force-distance curves was calculated for each of the set methodology to get the final adhesion value. Force-distance curves were calculated using the spring constant and sensitivity value of tip multiplied by the voltage values obtained in the line scan curves.

3.5 PDA Deposition on Fluorescent Beads

FluoSpheres Polystyrene Microspheres (10 μm, blue fluorescent (365/415) from Invitrogen were used for our study as a proof-of-principle. The concentration of these beads was around 3.6×10^6 beads/ml. To coat the fluorescent beads with PDA, 50 microliters of beads was added to 10 ml of 5mM tris HCl in which 5 mg of dopamine hydrochloride was added to get a 0.5 mg/ml PDA solution. It was left for shaking for an hour to allow the coating of PDA on the fluorescent beads. Once the coating process was done, it was centrifuged at 3000g for 20 min to get pellets of PDA coated beads. The supernatant was removed, and the PDA coated beads were washed 4 times to which 500 microliter of DI water was added (**Figure 8B**).

3.6 Fluorescence Evaluation using Plate Reader

The fluorescence spectra of coated and non-coated beads were observed to check if the coating of PDA on beads masks their fluorescence. A 50 microliter sample of beads (PDA-coated or non-coated) was taken and added to 450 microliters of DI water, since DI water does not result in any photobleaching [64]. Once the samples were ready, plate reader readings were taken to measure fluorescence emission.

3.7 Cell Viability Study

A Live/Dead assay (Invitrogen) was performed following the manufacturer's protocol using 2 cell types (macrophages and human umbilical vein endothelial cells (HUVECs)) to assess the viability of cells exposed to different PDA conditions.

3.7.1 Live/Dead assay with Macrophages for Preconditioned Media

For macrophages, 5×10^4 cells (RAW cells isolated from mice) were seeded per well in a 24-well plate (3 replicates per sample). The 2 test conditions were control and pre-conditioned media. On the same day, 3 PDA-coated cover slips were left dipped in media for 24 hours. The seeded cells were left to incubate for 24 hours after which the media in the wells was replaced with fresh media or the media conditioned with the PDA-coated cover slips. After 24 hours of culture under these conditions, the samples were removed and the Live/Dead stock solution that was prepared the same day was added to each well and left for incubation for 30 minutes. After 30 minutes the plate was taken for fluorescent imaging and the number of live and dead cells was manually counted.

3.7.2 Live/Dead assay with Macrophages with PDA-coated Beads

Again, 5×10^4 macrophages were seeded per well in a 24 well plate (3 replicates per sample) and left in the incubator for 24 hours. The 3 test conditions were control, non-coated beads and PDA-coated beads. After 24 hours, samples were prepared wherein 10 µl of beads (coated or non-coated) were added along with new media in each of the wells or just new media added to the wells of the control group. After 24 hours, the media was replaced with the live/dead stock and left to incubate for 30 minutes. The plate was then taken for fluorescent imaging and the number of live and dead cells was manually counted.

3.7.3 Live/Dead Assay with HUVECS for PDA-Coated Beads

The Live/Dead assay that was performed for macrophages was repeated using cultures of Human Umbilical Vein Endothelial Cells (HUVECs). HUVECs were seeded, grown and passaged in T75 plates until reaching 80-90 % confluency. Cells were maintained in Endothelial Cell Growth medium (Bio-Techne) replacing the media every 48 hours. Once the sufficient numbers of cells were grown, 5×10^4 cells were plated per well in a 24-well plate (3 replicates per sample) and left in the incubator for 24 hours and the same steps were repeated as were done for macrophages.

3.8 Fluorescent Bead Delivery Method Evaluation

For our study, application of the beads to the heart surface was achieved using a spray-on device. Before proceeding with the IVIS study, the spray pattern of the samples using the spray-on device was first optimized. For this, gelatin sheets were prepared and samples were sprayed onto them at different distances between the gelatin surface and the nozzle. The spray pattern was then checked for distribution of the sprayed bead samples. To make gelatin sheets, a hot plate was set at 40ºC after which a 10% w/v of gelatin Type A (175 strength) was prepared by allowing it to dissolve in the desired amount of water for an hour. After the gelatin solution was prepared, it was immediately poured into two 12-well plates. While preparing the bead samples, blue dye was added so that they could be more easily visible when sprayed onto the gelatin sheets. In the first plate, 3 µl of fluorescent beads (non-coated) was sprayed at 3 different nozzle distances of 1cm, 2cm and 4 cm and in the second plate 3 µl of PDA-coated fluorescent beads were sprayed at nozzle distances of 1 cm, 2 cm and 4 cm onto the prepared gelatin sheets. Once the

spraying was done, pictures of the spray patterns were taken and they were analysed in ImageJ and Origin to plot the 3-D surface plots, Intensity curves and FWHM values.

3.9 Assessment of Retention

After completion of the *in vitro* tests, further experiments were carried out with animal models to test the retention rate of the beads when applied to the surface of the heart. The non-coated fluorescent beads and the PDA-coated fluorescent beads were delivered into a specific region in the heart (left ventricle) of the animal models and their retention rate over a period of 24 hours was evaluated to check if the coating of PDA on the beads helps improve their retention.

3.9.1 Optimizing the Amount of Beads

The amount of beads needed for them to be visible by IVIS imaging was first optimized. Three different concentrations (10 µl, 30 µl and 50 µl) of non-coated beads and PDA-coated beads were sprayed onto harvested hearts and ex vivo IVIS images were taken. The amount of beads which gave comparable and significantly better fluorescent images were considered to be used for further experiments. This consideration was taken into account as these beads had to be easily detected *in vivo* in further experiments making it important to take a sample amount appropriate for the imaging steps.

3.9.2 Animal Experiments

All animal experiments were first approved by the University of Ottawa Animal Care Committee (ACC) and were performed in accordance with the National Institutes of Health Guide for the Care and Use of Laboratory Animals.

3.9.3 Animal Model

For the *in vivo* studies, 8-10 week oldC57BL/6 mice were anesthetized (2% isoflurane and 1 dose of 1.2 mg/kg of SR buprenorphine) and intubated. The heart was then exposed via a small left thoracotomy procedure.

3.9.4 Delivery of Beads and PDA-Coated Beads using Spray-on Device

Under light anesthesia (1-2% isoflurane via nose cone), the non-coated or PDA-coated fluorescent bead applications were delivered via the spray-on device onto the surface of

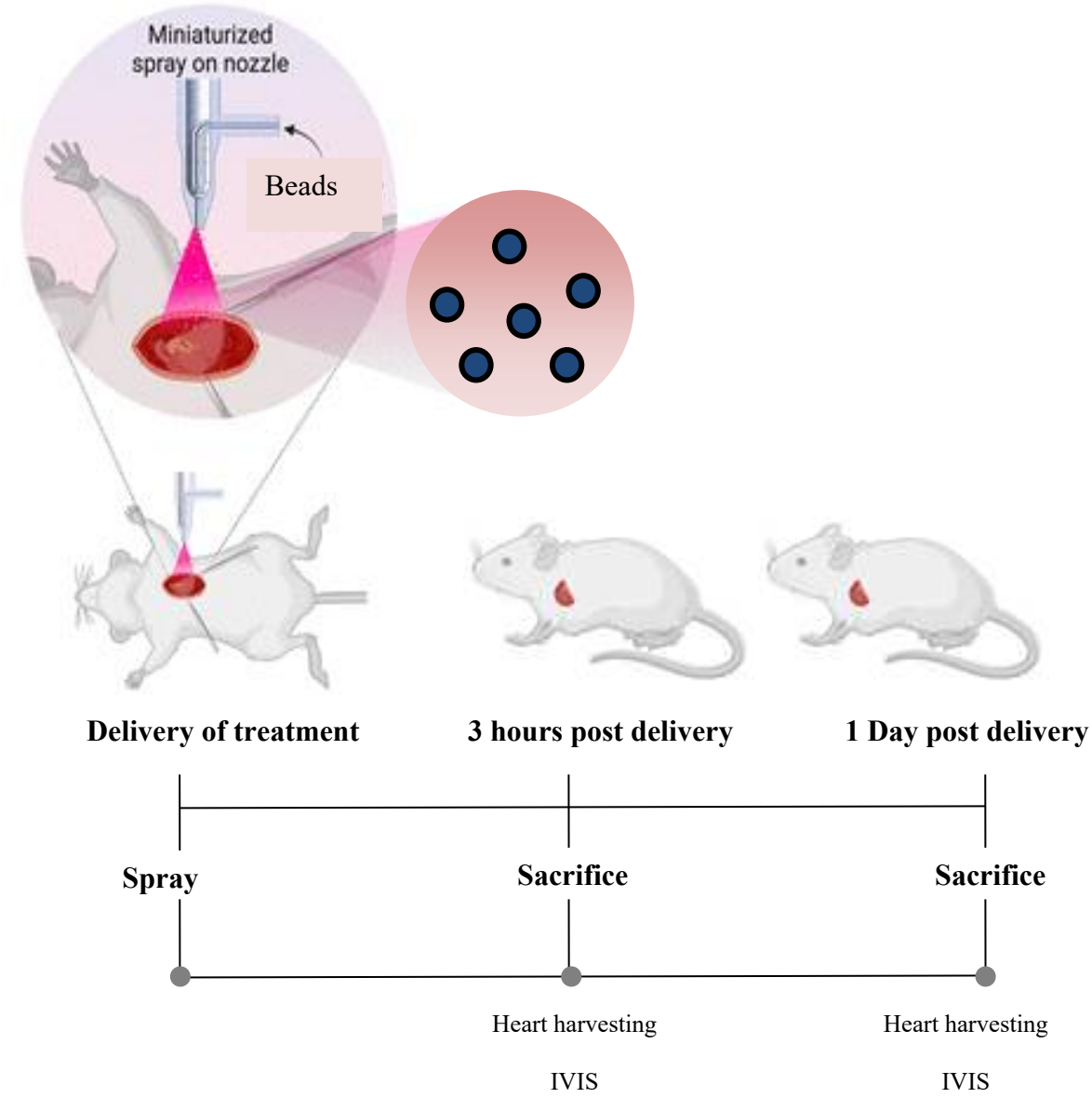

Figure 9. Schematic of in vivo study timeline on mouse model treated with non-coated and PDA-coated beads

The treatments were delivered via a spray-on device, and bead retention was assessed by IVIS imaging at 3 hours and 1 day after application [65].

the heart. Once the treatments were sprayed, the chest was closed. Mice were randomly divided into four groups (n=4 mice per group) to receive a spray-on treatment consisting of: non-coated fluorescent beads (evaluated at 3 hours), non-coated fluorescent beads (evaluated at 1 day), PDA-coated fluorescent beads (evaluated at 3 hours), PDA-coated beads (evaluated at 1 day). At 3 hours post spraying the treatment, 2 groups of mice were sacrificed: the non-coated fluorescent bead (3 hours) and the PDA-coated fluorescent bead (3 hours) groups. After sacrifice, the hearts were extracted and stored in PBS for IVIS imaging. The stored hearts were taken for *ex vivo* imaging to check the localization and area of spread of the sprayed treatments. After 1 day, the remaining two groups of mice were sacrificed and the hearts were harvested and stored for IVIS imaging (**Figure 9**).

3.9.5 Assessment of Retention Rate using IVIS

The extracted hearts were taken for IVIS imaging by a PerkinElmer IVIS Spectrum system using Living Image software. The region of interest (ROI) was identified and measured for each heart (λ excitation: 400 nm; λ emission: 740 nm). The images were collected using the epi-illumination feature, whereby the fluorescence reading is taken from the surface of our heart samples. For our studies, we used auto exposure to acquire the sequence. Once the images were captured and displayed by the software, the circle ROI was placed and used to measure the radiant efficiency values within the selected area and these values were then used to measure and compare the retention rate values. As a positive control group, untreated hearts were collected, and the spray-on application of fluorescent beads was performed *ex vivo*. These were immediately imaged by IVIS and used to represent 100% bead retention. The data was reported as relative radiant efficiency (%) and normalized to the positive control hearts.

3.10 Statistical Data Analysis

Statistical analysis was performed using ANOVA test. Post hoc comparisons were performed using a t-test assuming equal variances to compare the means of the different groups. All the results are expressed as mean ± standard deviation and results were considered significant for $p<0.05$.

CHAPTER 4

Results and Discussion

4.1 Structural Analysis

In order to probe structural characteristics, we used SEM to study the homogeneity of the surface of the PDA coatings and AFM for all the different deposition conditions. The main aim was to find the optimal deposition time for a PDA coating that would result in the maximum adhesion force. Before moving ahead with AFM, SEM was used as a preliminary approach to see the structure of the PDA coatings. The SEM images of all the substrates showed that the surface of the PDA coating in case of Tris5mM exhibited less granular structures as compared to that of the Tris10mM and Tris15mM recipes. Next, different pH conditions were evaluated for coating using the Tris5mM and Tris10mM recipes. SEM images were taken for pH5, 7 and 8.5, wherein pH5 and pH7 coatings showed the formation of aggregates of PDA which is not seen when a pH of 8.5 was used. PDA is a zwitter ion molecule as it has both acidic (catechol) and basic (amine) groups. The isoelectric point of PDA is 4 [66]. When the solution pH is acidic, it leads to a total positive surface charge due to the presence of protonated amines and a negatively charged PDA due to the deprotonated catechol groups at a higher pH [67-68]. As per the initial study of PDA deposition [69], a pH of 8.5 was superior since it facilitated the polymerization of PDA which allows for the autooxidation of dopamine hydrochloride by air. In the reaction steps in the formation of PDA, the state where there is a reaction between PDA and PDA-quinone, it is important to shift the balance of the reaction towards the right in order to produce more quinone units as the higher number of quinone moieties will improve the ability of linkage for the biomolecules and the shift in this balance occurs because of basic conditions. Thus, a more homogenous coating at pH 8.5 and formation of aggregates at lower pH may be attributed to the occurrence of a successful and spontaneous PDA deposition due to auto oxidation. The same conditions

(pH 8.5) were then tested with deposition times of 30 minutes, 2 hours and 3 hours. The SEM image of the coverslip which was coated for 30 minutes showed less granular structures owing to the reduced time for the polymerization of PDA. However, the surface for coverslips with 2 hours and 3 hours of deposition time showed a highly uneven structure (**Figure 10A-D**). The SEM results that we got were similar to the ones that were previously published [70] showing the formation of granules and aggregates with the increase in reaction time. Based on our results and previous studies, it was decided that a PDA protocol with tris 5mM as solvent at pH 8.5 gave a more homogenous surface, and these values were used in all subsequent experiments.

Since the aim of our optimization study was to find a deposition time with the maximum adhesion force, it was decided to take AFM readings for the most even and homogenous surface coating without any presence of PDA aggregates and vary the deposition times and compare adhesion forces for each of them. For each of the deposition times tested, force distance curves were plotted (**Figure 10E**) and an average of 180 force distance scans was taken for each deposition time. Adhesion force from each of the force-distance curve was calculated by taking the difference of the lowest point on the curve and the flat line on the curve. The average adhesion force for a deposition time of 1 hour was found to be 216 ± 152 nN which was greater than that of other deposition times. For the deposition time of 30 minutes, the adhesion force was found to be 159 ± 77 nN. The lower adhesion force may be attributed to the insufficient PDA deposition in a lesser time frame thus resulting in an uneven coating on the surface; there might be areas on the coverslip surface where the coating of PDA has not been achieved in 30 minutes thus leading to a lower adhesion force. For deposition times greater than 1 hour, the adhesion force decreased with an increase in time with values of 177 ± 156nN and 147 ± 143 nN for 120 minutes and 180 minutes, respectively. However, no significant difference in the adhesion force was observed between deposition times with huge standard deviation values, despite the observed trend (**Figure 10F**). This result may be attributed to the formation of aggregates as the deposition time increases beyond 1 hour, which might reduce the adhesion force that the PDA coating exerts. As shown in the SEM images of our study and also in other studies, the size of the insoluble PDA aggregates that precipitate during the coating procedure increases with deposition/polymerization time [71].

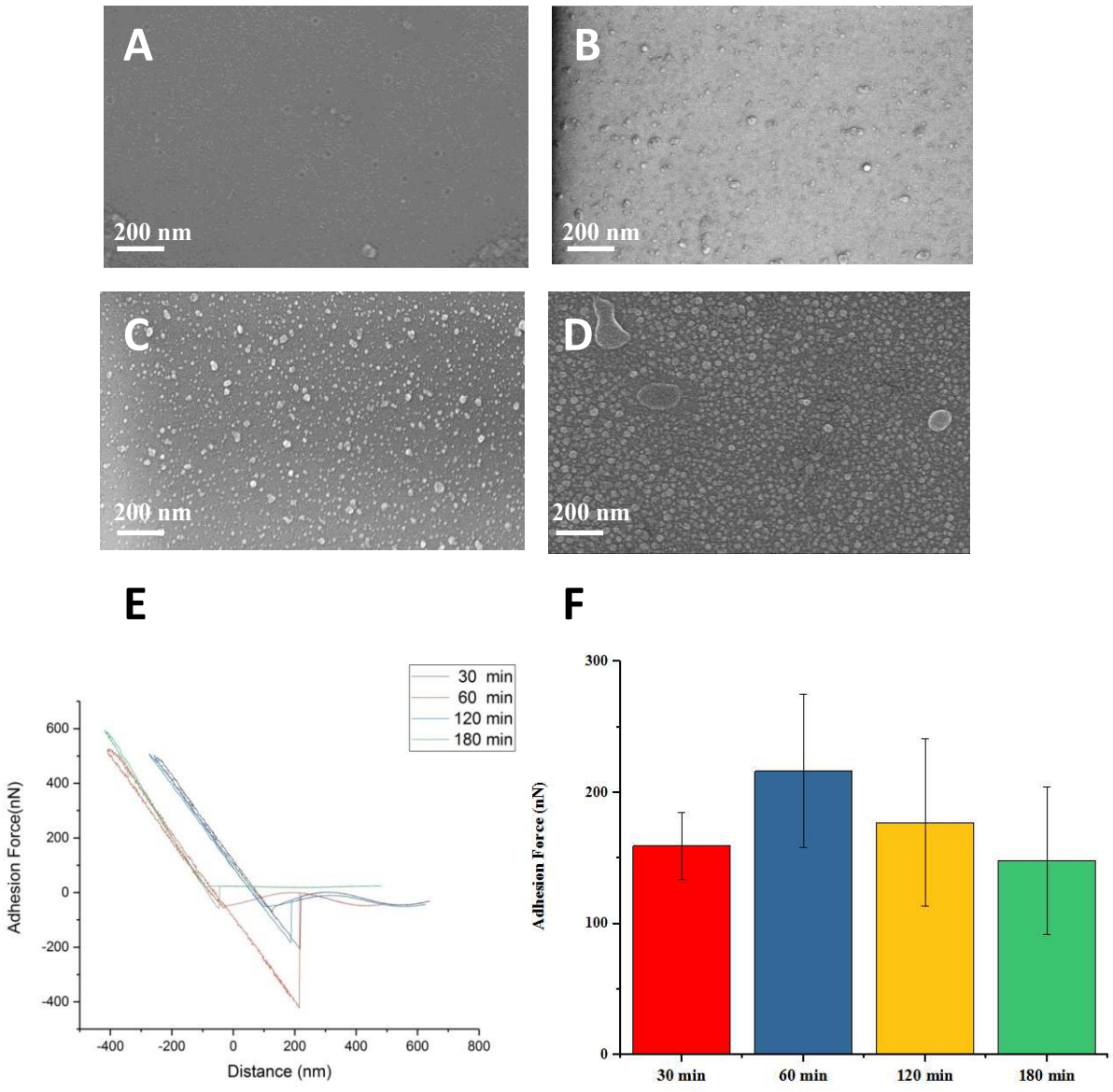

Figure 10. Structural analysis of PDA-coated coverslips using SEM and AFM

SEM images of PDA coatings with deposition times of A) 30 minutes B) 60 minutes C) 120 minutes and D) 180 minutes. E) Representative force-distance curves for deposition times of 30, 60, 120 and 180 minutes. F) Plot of adhesion force calculated for 180 curves per sample with no significant difference found between the deposition times (ANOVA test with Tukey analysis; n=3)

These by-products of PDA precipitates have weak adhesion capability and do not contribute to surface modification [72], and our study showed similar results as well. However, the difference in the adhesion forces among the different deposition times is not significant as per the statistical data analysis that was done indicating that the difference in deposition times up to 3 hours does not make that great of a difference in the adhesion forces. Considering previous studies and the homogeneity of the surface and the adhesion force as per the SEM and AFM results in our study, one standard value of 0.5 mg/ml of PDA in tris buffer at a pH of 8.5 and a deposition time of 1 hour was used to get a thin and homogenous film with comparable adhesion force that was used for all further experiments with fluorescent beads.

This value was then translated to the coating of spherical beads for further tests. It has been seen in previous studies that PDA retains its properties found on plane surfaces even on spherical particles [73]. Based on these studies, we moved ahead with the results obtained on glass coverslip to translate this to spherical microparticles with the belief that PDA will have the same adhesion properties after coating them on fluorescence beads as found on the glass coverslip. Previous results with PDA hydrogels have shown that they exert similar and comparable adhesive strength to almost all types of surfaces including glass, rubber, biological organs like heart, spleen, kidney, lung, liver and even human skin, thus indicting the adhesiveness of PDA irrespective of the surface properties of the substrate [74]. Also, it was shown that particles, whether nano-sized or micro-sized, retain their properties after getting wrapped by PDA [73]. This provided a solid rationale for the use of PDA to coat nanoparticles in the future with the goal of enhancing their efficacy for therapeutics delivery to the infarcted myocardium.

4.2 Physiochemical Analysis

The inherent fluorescence of the beads can be used to detect and track their location once they are injected into the animal model. Therefore, it was important to make sure that we still had detectable fluorescence after coating with PDA. In order to probe this, we used fluorescence spectroscopy to compare the fluorescence of coated and non-coated beads at different excitation wavelengths of 400 nm, 550 nm and 600 nm. In all cases, visible fluorescence was detected in PDA-coated beads, although it was significantly lower than that of the non-coated beads (**Figure 11A-B**). The relative fluorescence units (RFU) for

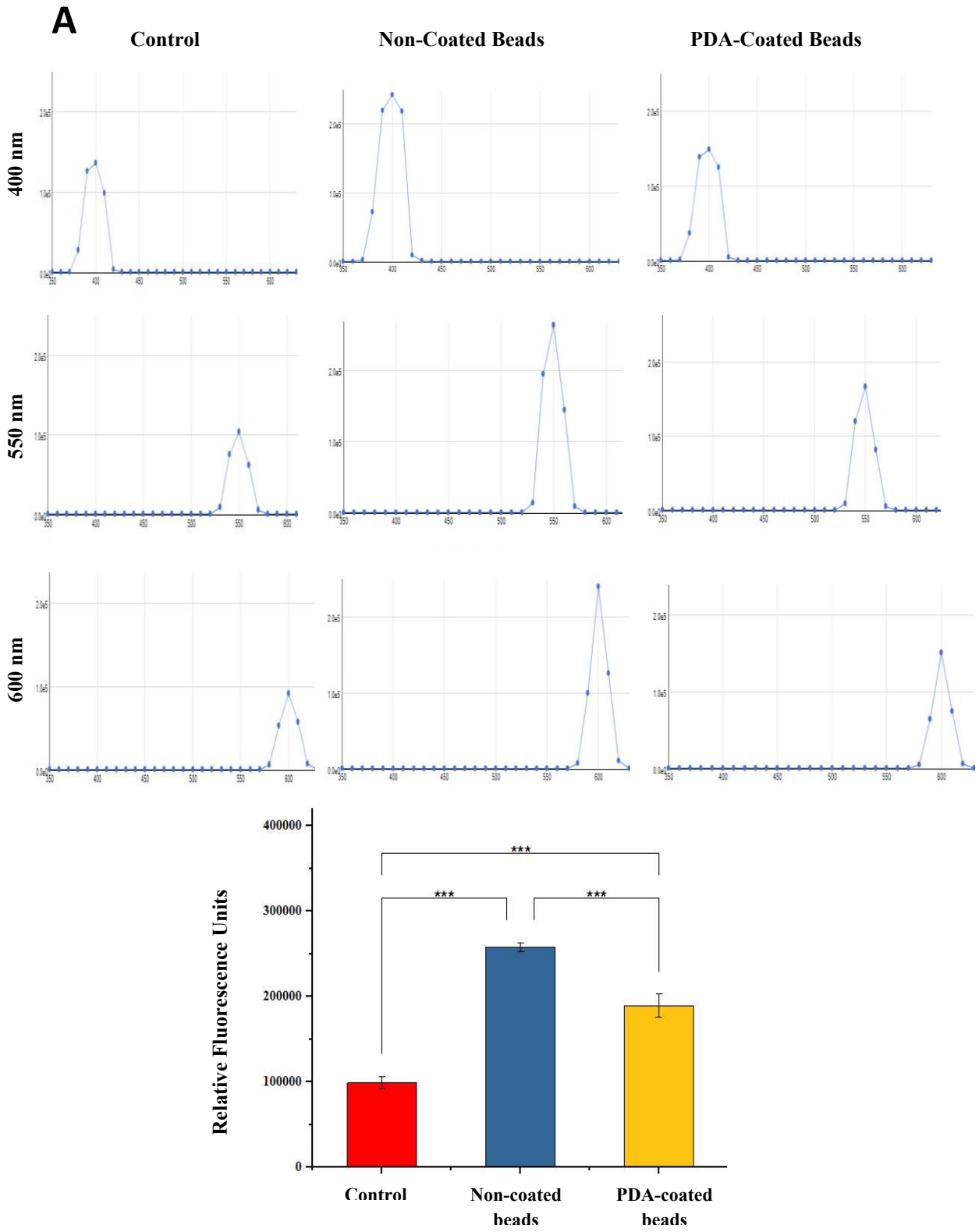

Figure 11. Physiochemical analysis of non-coated and PDA-coated beads

A) RFU plot of control, non-coated and PDA-coated beads at excitation wavelengths of 400 nm, 550 nm and 600 nm. B) RFU of PDA-coated beads is lower than that of non-coated beads showing that PDA coating does lower fluorescence intensity, but it is greater than control indicating the detection of fluorescence even after coating, ANOVA Tukey Analysis (***=$p<0.001$).

beads wrapped with PDA was significantly lower than the non-coated beads ($p<0.001$). Despite this, the RFU for coated beads was significantly greater than that of the control ($p<0.001$). These results indicated that the beads still retain their fluorescent properties even after PDA coating, albeit with somewhat lower intensity. Previous studies on PDA coating on nanoparticles have shown that they retain their properties, making it possible to utilize the properties of both the nanoparticles and PDA as well [73].

4.3 In vitro Cell Viability

4.3.1 Macrophage Cell Viability

To evaluate the biocompatibility of the PDA-coated beads, an *in vitro* Live/Dead assay was performed using macrophages (**Figure 12A-D**).The cytotoxicity was evaluated for both non-coated beads and PDA-coated beads as it was important to differentiate between any cytotoxicity contributed by the beads themselves versus that of the PDA coating. The live/dead images were taken 24 hours after the addition of bead samples to the macrophages. Prior to performing the Live/Dead assay with cells in direct contact with the beads, preconditioned media studies were done. To this end, media was added to a PDA-coated coverslip for 24 hours, after which the same media was removed and added to the macrophage cultures to see if there are any PDA residues in the media that could be cytotoxic. The cell viability in case of preconditioned media was 90.3%, which was not different compared to the viability of 94.5% observed for the control samples ($p>0.05$). After this, the Live/Dead assay was carried out with non-coated and PDA-coated beads where they were added directly to the media of cultured macrophages for 24 hours. The images revealed that cells treated with non-coated beads had a viability of 94%, which was not significantly different compared to the 97% cell viability observed for the control. The viability of macrophages treated with PDA-coated beads was found to be 93%, which was significantly lower than that of control ($p<0.05$). However, there was no difference in viability between coated and non-coated bead treatment, and both were above 92% after 24 hours. This indicated that both the samples were biocompatible and posed no significant toxicity concern to cells or tissues.

4.3.2 HUVEC Viability

The same viability experiments were repeated using HUVECs to better confirm cytotoxicity potential before moving to *in vivo* tests. The Live/Dead assay for HUVECs revealed very similar results as was seen with macrophages (**Figure 13A-D**). HUVECs treated with non-coated beads showed a viability of 96%, which was not different from the viability of 98% seen for control. For HUVECs treated with PDA-coated beads, viability was found to be 95% significantly, which was significantly reduced compared to control ($p<0.01$). The viability in all groups was more than 93% in all the repeats taken indicating no significant toxicity concern to cells after 24 hours of incubation. These results were similar to those earlier reported, which concluded that PDA does not exhibit any harmful effects on the cells viability and function. It has also been reported that PDA-coated nanoparticles stay intact even after 24 hours incubation [76]. Apart from its own biocompatibility results, it has been shown that a coating of PDA can lower potential toxicity of other biomaterials. One such study looked at the effect of a PDA coating on quantum dots and poly(L-lactic acid) (PLLA). Even though quantum dots have demonstrated suitability for drug delivery, cancer targeting and many other biomedical research applications, they still have some limitations, with cytotoxicity being potentially the most concerning, as this toxicity may lead to the occurrence of vascular thrombosis [77]. The same holds true for many other biomaterials, including PLLA, which can promote significant tissue inflammation. PDA coatings have been shown to reduce tissue inflammation as well as blood immunogenicity of such biomaterials, and this occurs due to the presence of protein adsorption and metal chelation by PDA [78].

4.4 Evaluating the Spray Patterns

Before the *in vivo* experiments, the sample spray application was optimized by evaluating different spray volumes and distances and assessing spray patterns and surface morphology. There was no statistical difference between the FWHM of the sprayed pattern for different amounts of sample sprayed in both non-coated and coated samples (**Figure 14, Figure 15**). In contrast, the spray distance did have an effect on the spray pattern observed. Specifically, the diameter of the sprayed sample on gelatin sheets was found to be around 8mm when a nozzle distance of 1 cm was used compared to diameters of around 10 mm and 11.5 mm for nozzle distances of 2 cm and 4 cm, respectively. The circular diameter of the sample sprayed from a nozzle distance of

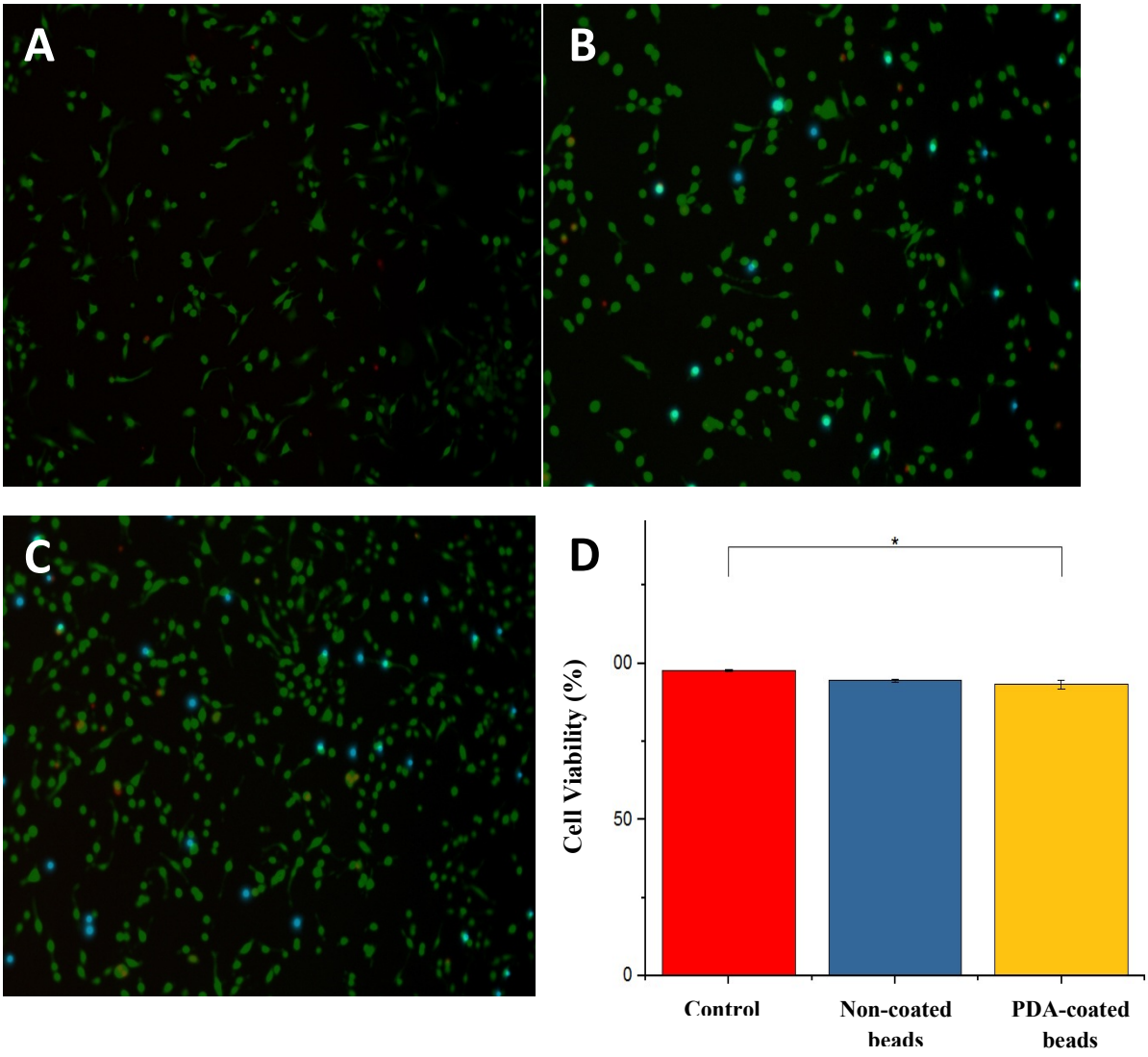

Figure 12. Cytotoxicity Assay with Macrophages over 24 hours

Live/Dead images of macrophages 24 hours after treatment with: A) control, B) non-coated beads, and C) PDA-coated beads using magnification = 20X D) Cell viability after 24 hours of incubation (ANOVA Tukey analysis; *$p<0.05$)

1 cm was approximately the same as that of a standard infarct size in the surgically induced MI mouse heart, suggesting that a spray from 1 cm will appropriately cover the entire therapeutic target area.

After determination of the ideal nozzle distance, the amount of sample to be sprayed was then optimized. For this evaluation, three different amounts of samples (5 µl, 10 µl and 15 µl) were sprayed on to *ex vivo* organs fixed in 4% PFA to take IVIS readings. Once the samples were kept in the chamber, different specifications were set and IVIS images viewed using the Living Image software. The IVIS readings were taken at an excitation wavelength of 400 nm and an emission wavelength of 520 nm, (the sample height was 0.5 cm, an aperture of 2 F/stop was used and binning was set to medium). After obtaining the IVIS images, the radiant efficiency was measured by using the ROI tool for all the samples. A circle was chosen as a ROI tool and the same ROI was used to find the radiant efficiency values for the same selected areas on each of the heart samples. As per the ROI measured for both non-coated and PDA-coated nanoparticles (**Figure 16A-C**), it was observed that the radiant efficiency for the sample volume of 10 µl was found to be greater when compared to that of the sample volumes of 5 µl and 15 µl (**Figure 16D**; $p<0.05$) and similar results were observed for PDA-coated beads as well (**Figure 17A-D**). The sample size of 5 µl was too small to obtain reliable detection by IVIS and to proceed to further *in vivo* experiments. When a sample size of 15 µl was used, it was observed that the sprayed sample spread beyond the target area, suggesting that a larger sample volume would also not be appropriate for the *in vivo* experiments to follow. Thus the 10 µl of sample was selected for further experimentation as it demonstrated excellent radiant efficiency and localized to the desired target area. When performing IVIS imaging it is important to consider that most organs and tissues will exhibit some level of autofluorescence. The autofluorescence of the host tissue can possibly hinder differentiation of the fluorescence emitted from the sprayed sample. For this reason, a sprayed sample that has an easily detectable radiant efficiency (as shown with the 10 µl sample) will be better suited for localizing and quantifying the treatment application.

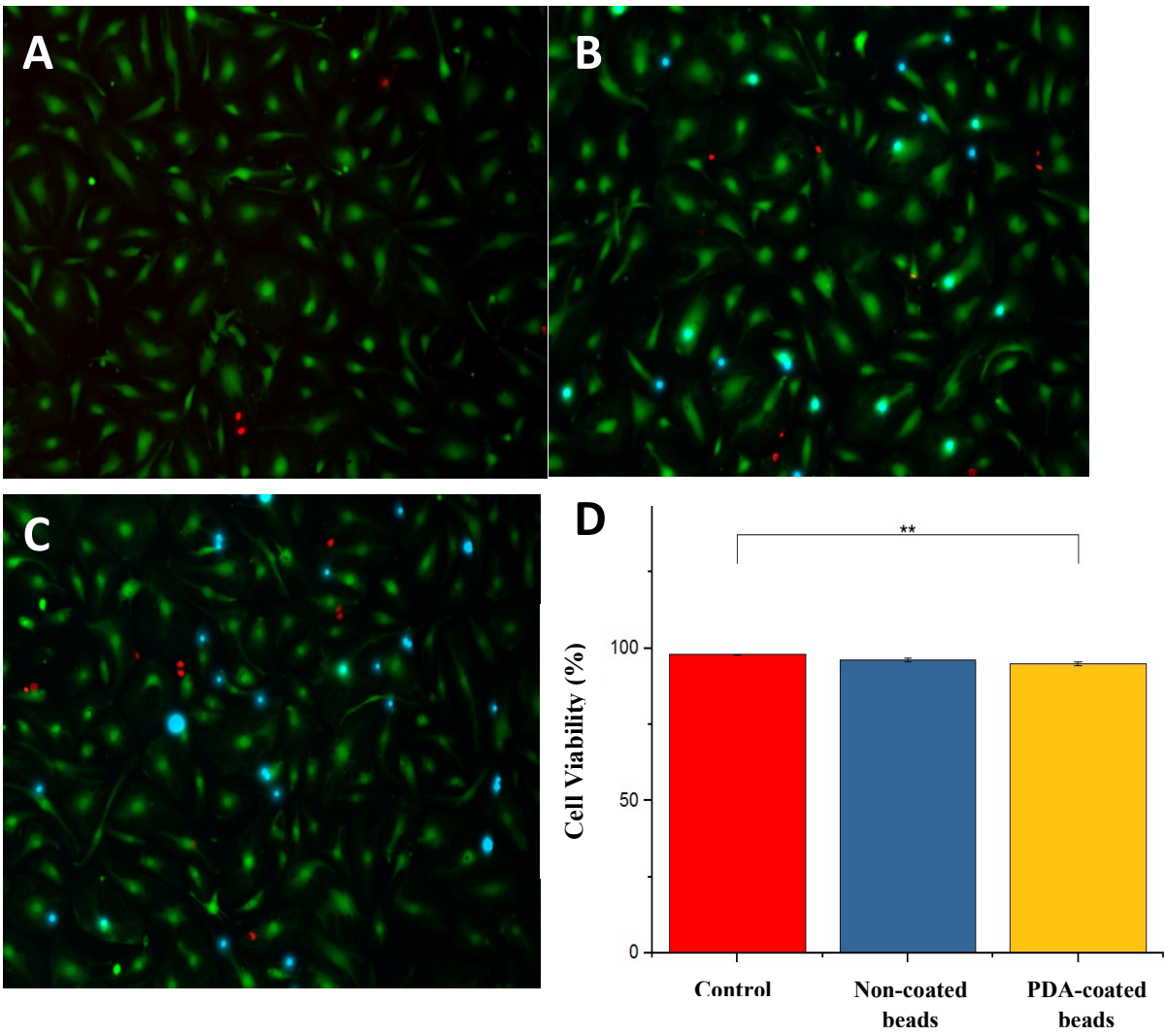

Figure 13. Cytotoxicity Assay with HUVECS over 24 hours

Live/dead images of HUVECs 24 hours after treatment with A) control B) non-coated beads and C) PDA-coated beads using magnification = 20X D) Cell viability after 24 hours of incubation(ANOVA Tukey analysis, **p<0.01)

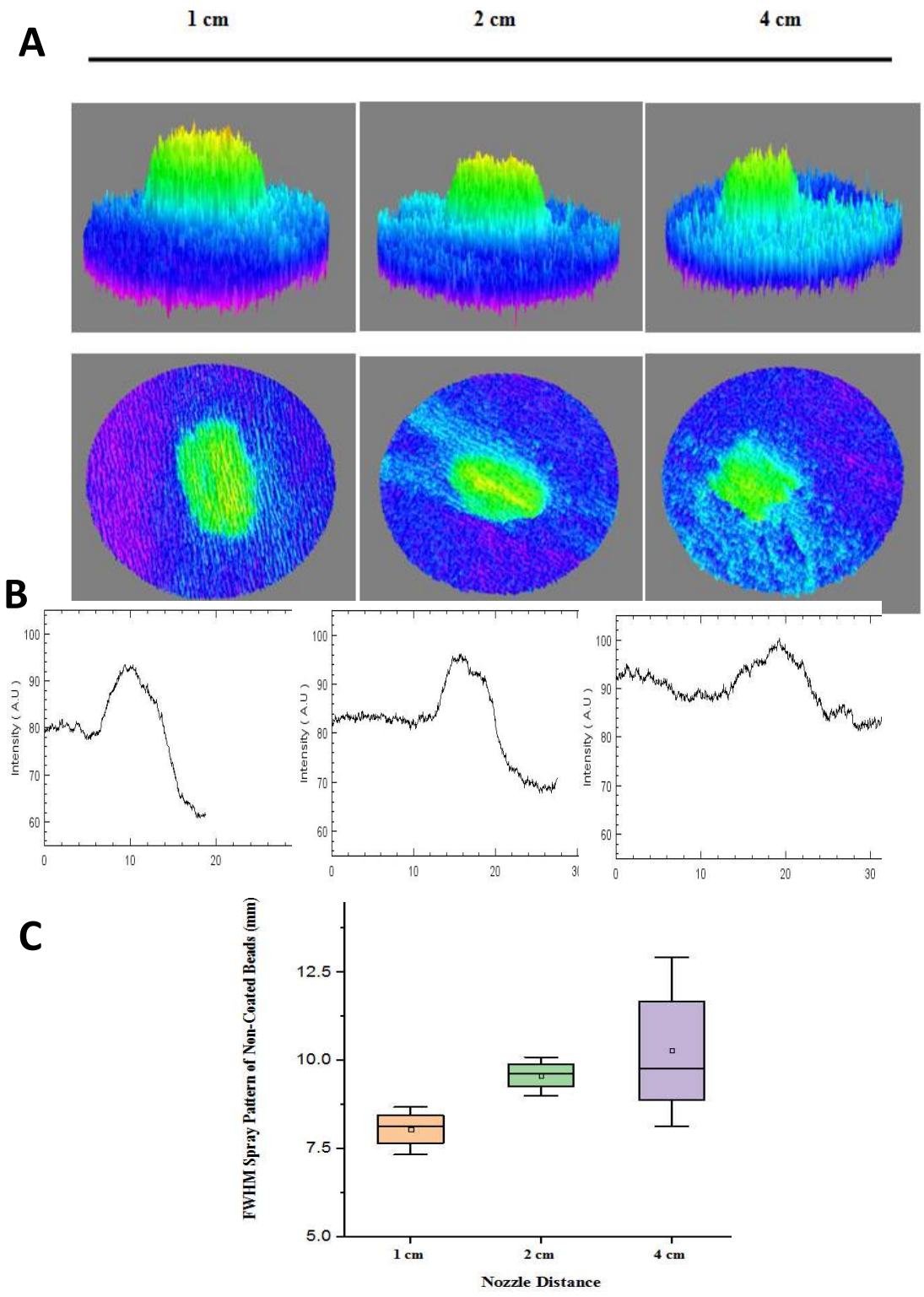

Figure 14. Spray-on optimization for non-coated beads

A) 3D surface plots illustrating the intensity of spray patterns as measured using ImageJ. B) Intensity profile of a transverse section of the spray pattern. C) Full width half maximum of the spray patterns as measured from the profile plots.

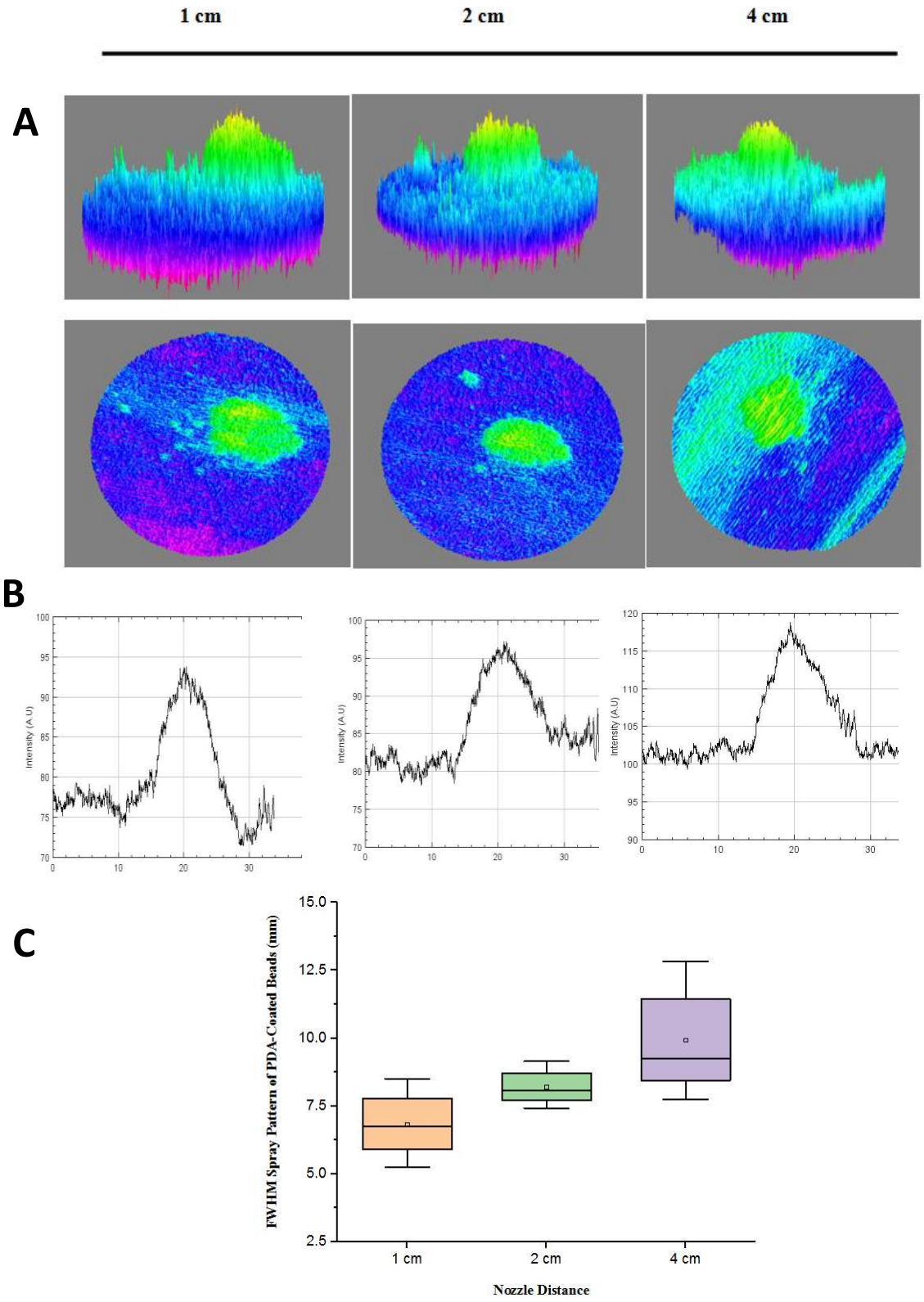

Figure 15. Spray-on optimization for PDA-coated beads

A) 3D surface plots illustrating intensity of spray patterns as measured using ImageJ. B) Intensity profile of a transverse section of the spray pattern. C) Full width half maximum of the spray patterns as measured from the profile plots.

4.5 Retention Rate Evaluation for the PDA-coated Beads

The following *in vivo* experiments were all carried out using a nozzle distance of 1 cm and a sample size of 10 µl. The *ex vivo* hearts were not fixed after harvest and IVIS images were taken immediately after animal sacrifice. Images taken at an emission wavelength of 520 nm showed autofluorescence and made it difficult to track the location of the beads. To eliminate the autofluorescence from images, the emission wavelength was increased to 740 nm so as to get more precise images of the spray-on application (**Figure 18**). The retention of the beads was evaluated over a period of 24 hours by comparing the radiant efficiency of sprayed samples relative to a 100% retention control. For this experiment, the control with 100% radiant efficiency consisted of a heart sprayed with the beads *ex vivo* and imaged by IVIS immediately after spraying. The relative radiant efficiency with respect to control for non-coated beads at day 1 was 64%, which was significantly lower ($p<0.01$) than its retention of 85% seen at 3 hours (**Figure 19A)**. This indicates a decrease in the amount of sprayed sample of non-coated beads over a 1-day period. However, in the case of PDA-coated beads, the radiant efficiency was 86% and 79% after 3 hours and 1 day, respectively, indicating that there was no loss of the beads from the surface of the hearts over this time. The loss of non-coated beads can likely be attributed mostly to extrusion forces of the pumping heart causing the particles to be washed away to off-target sites. However, the same was not seen in the case of the PDA-coated beads, suggesting that the adhesive PDA coating helps improve retention by limiting the loss of the particles due to physical forces. The adhesive beads can now stick to the heart surface against the internal forces. Previous results have demonstrated the adhesiveness of PDA with cells and tissues, where PDA enhances cell adhesion on the coated surfaces. This has been attributed to the PDA reacting with the serum proteins that have amines or thiol molecules via Michael addition or Schiff base chemistry [79]. Since serum proteins help in cell adhesion, the reaction between the serum proteins and the PDA surface may enable better adhesion of the cells. Based on the radiant efficiency, retention rate was measured over 1 day by finding out what percentage of beads seen at 3 hours is still present at 1 day. Non-coated beads were found to have a retention rate of 76% significantly lower than that of PDA-coated beads which was found to be 92%($p<0.01$) (**Figure 19B)**. This difference in the retention rate confirms the additional adhesiveness conferred by coating the beads with PDA.

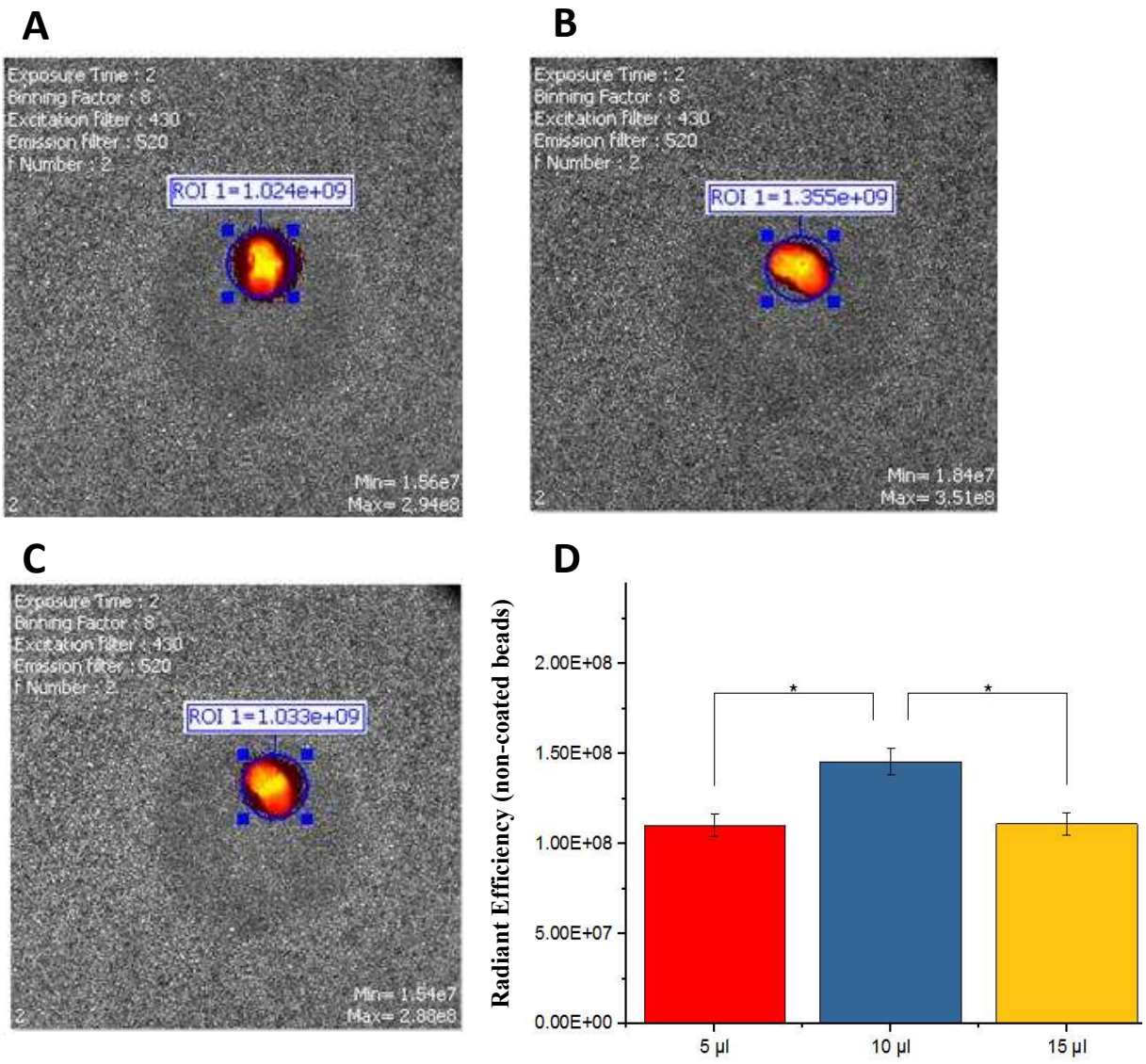

Figure 16. IVIS images for spray-on optimization for non-coated beads

IVIS images showing radiant efficiency values using ROI tools after spraying non-coated beads onto ex vivo fixed organs with different sample amounts of A) 5 µl B) 10 µl and C) 15 µl. D) Plot of radiant efficiency for sample sprayed with 10 µl beads showing the maximum intensity compared to that of 5 µl and 15 µl (ANOVA with Tukey posthoc analysis; *$p<0.05$; n = 3).

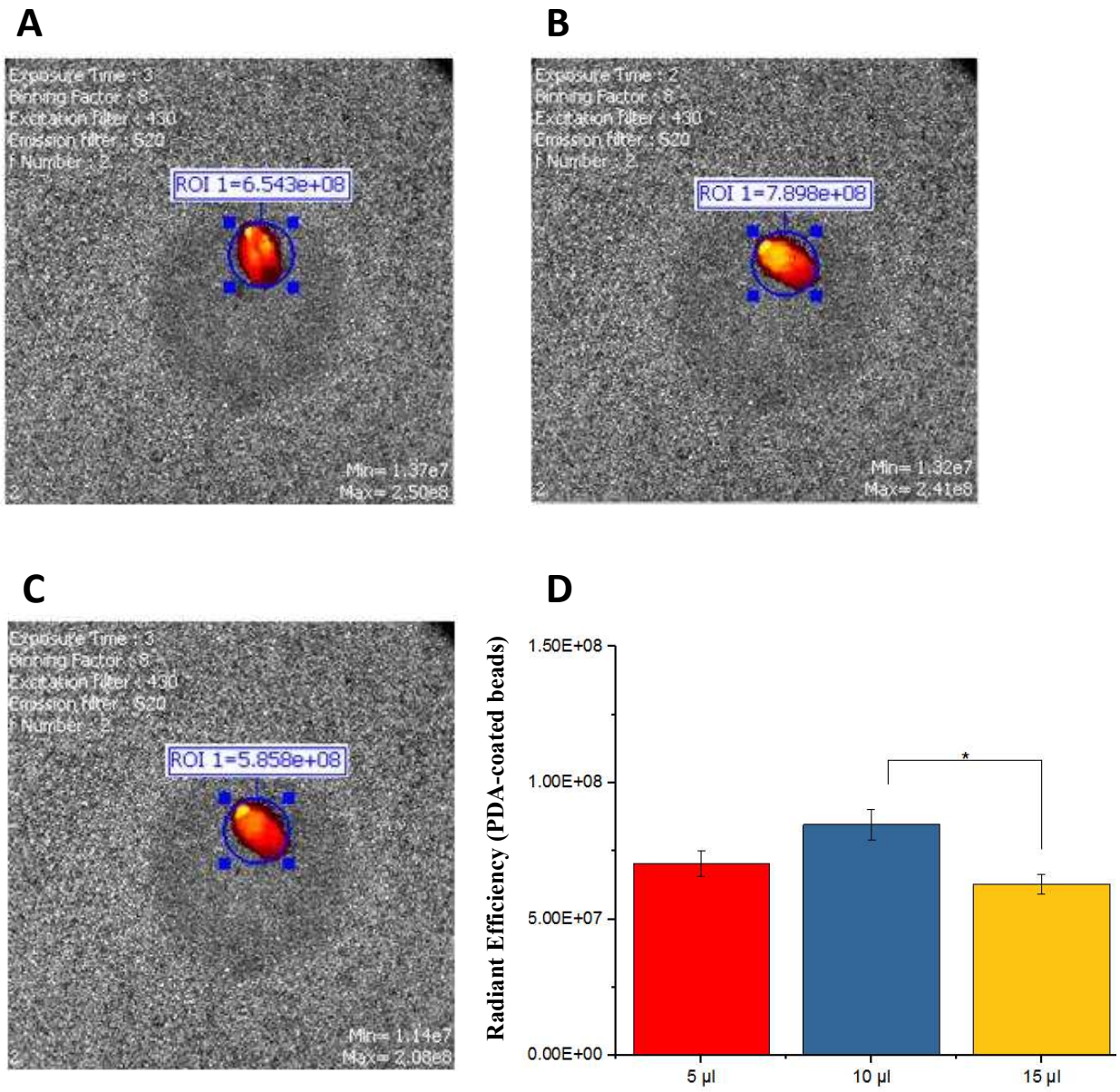

Figure 17. IVIS images for spray-on optimization for PDA-coated beads

IVIS images showing radiant efficiency values using ROI tools after spraying PDA-coated beads on ex vivo fixed organs with different sample amounts of A) 5 µl B) 10 µl and C) 15 µl. D) Plot of radiant efficiency for sample sprayed with 10 µl beads showing the maximum intensity compared to that of 5 µl and 15 µl (*$p<0.05$, n = 3).

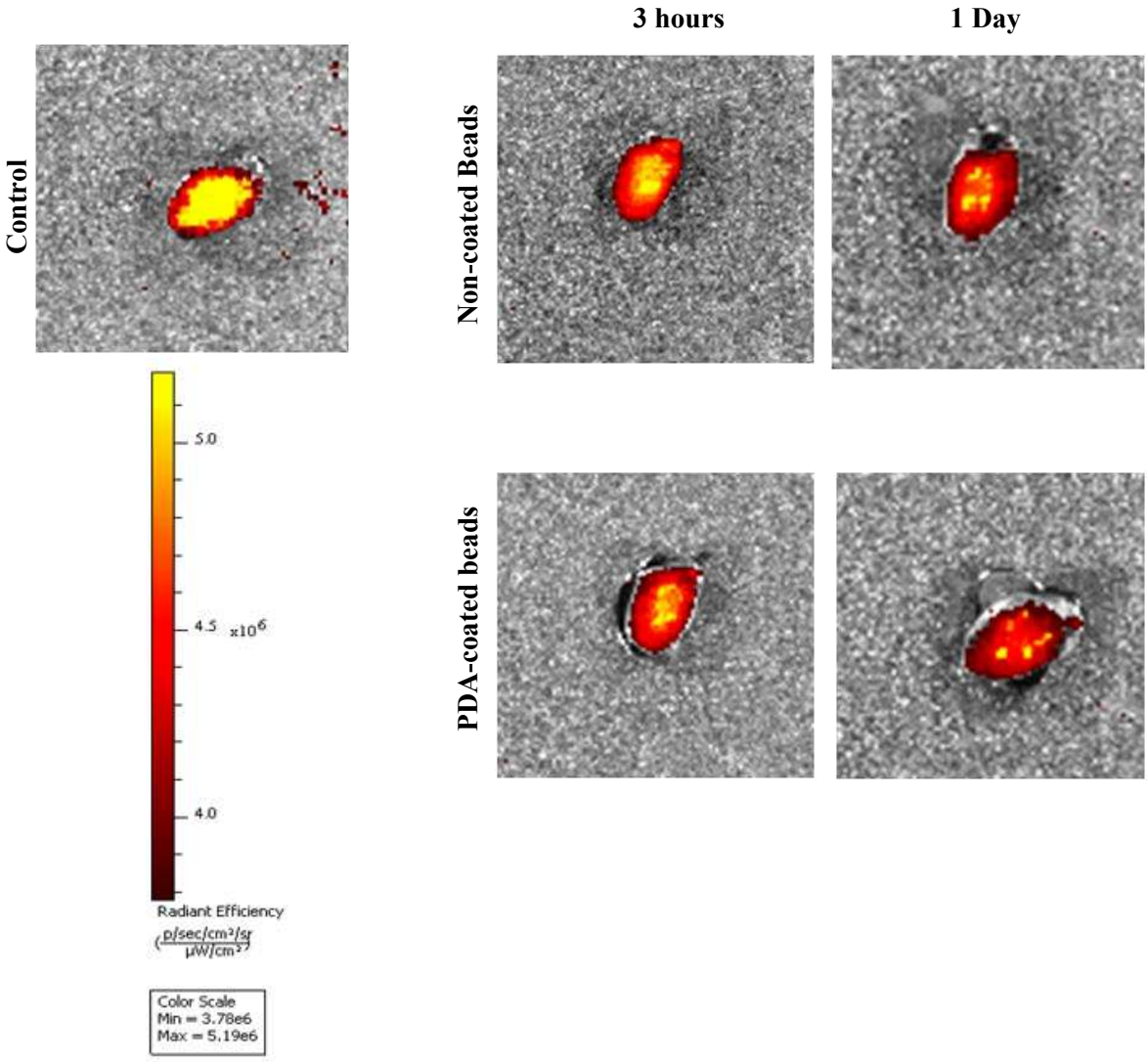

Figure 18. IVIS images for in vivo experiments

IVIS images for hearts that received spray-on application non-coated or PDA-coated beads at 3 hours and 1 day. The 100% control consists of an ex vivo heart that was imaged immediately after receiving spray-on treatment.

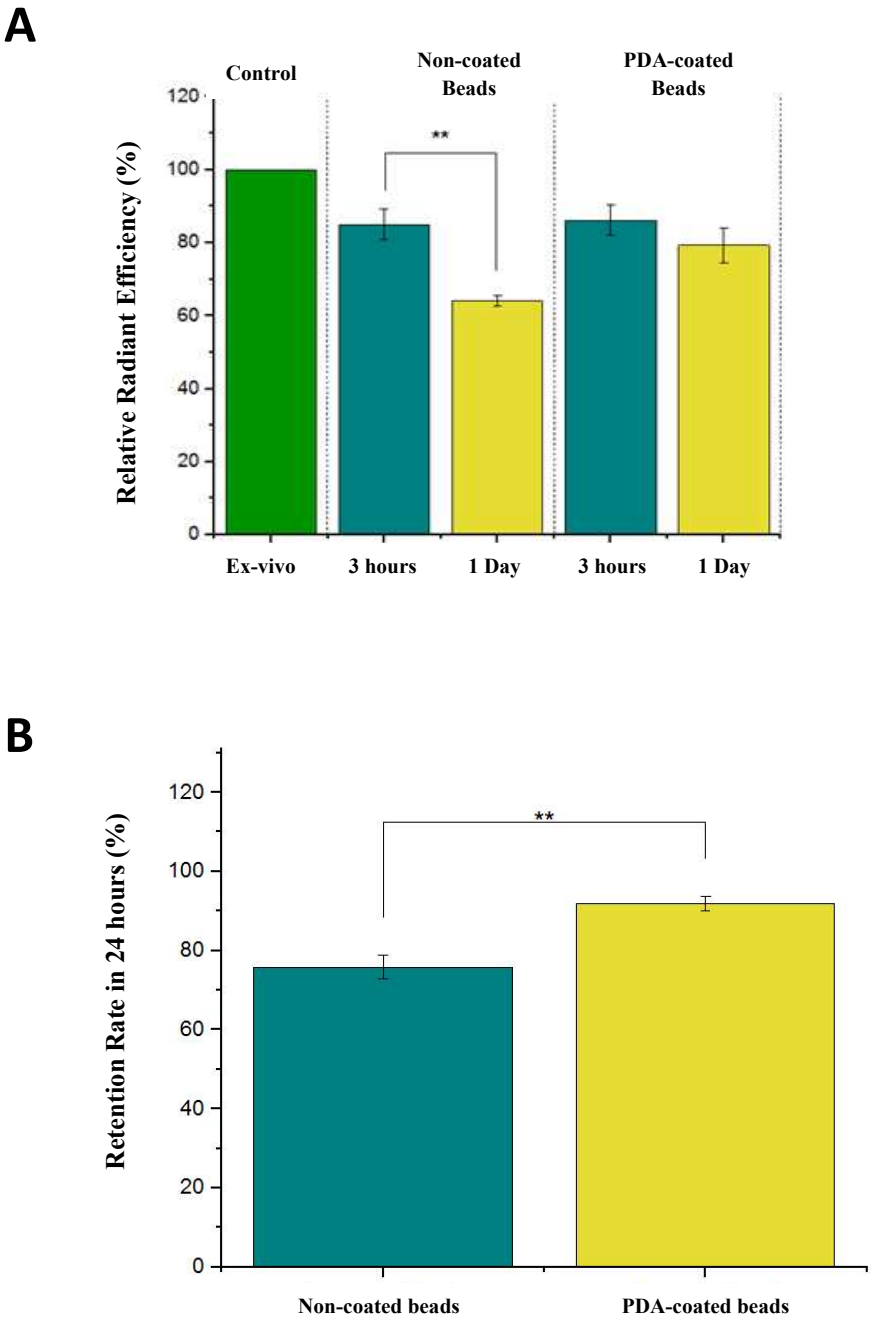

Figure 19. Retention rate evaluation for in vivo experiments

A) Relative radiant efficiency normalized to control. B) Retention rate calculated over 24 hours found to be greater in PDA-coated beads (**$p<0.01$, $n = 4$)

In summary these results provide novel insight into the use of PDA as an adhesive coating that can be used to modify the surface and improve the retention of any nanoparticles for biomedical use. Specifically, our findings support the use of PDA coatings and their further study for the modification of delivery vehicles for applying therapeutic agents post-MI.

CHAPTER 5

Conclusion and Future Directions

The first part of the study was mainly focused on determining any correlation between the time allowed for dopamine polymerization to deposit a layer of PDA on the surface and the adhesion force of the formed coating. As per previous studies and the results of scanning electron microscope, a PDA coating obtained at a pH of 8.5 in a solvent of 5mM Tris HCl and at a dopamine hydrochloride concentration of 0.5 mg/ml was found to have a homogenous coating as compared to other values. Additionally, this formulation exhibited very few to no PDA aggregates as determined by SEM. It was also observed that increasing the deposition time led to the formation of PDA aggregates on the surface and an increase in the deposition times resulted in a decrease in homogeneity of the PDA coating. The adhesion force was not significantly different between the coatings with different deposition times. However, a trend for reduced adhesion force with increased deposition times was observed. This was in line with the increase in aggregate formation with higher deposition times. So, a correlation might be possible between the amount of PDA aggregates formed on the substrate and the adhesion force between them.

The second part of our study was to get a proof-of-principle for the use of the PDA coating to increase nanoparticle retention before moving ahead with the application of therapeutic nanoparticles in an MI model. This study assessed the ability of a PDA coating to increase the adhesive strength and retention of commercially available fluorescent particles when applied to mouse hearts. We started with proving that the fluorescence intensity of the particles is maintained after the coating process. It was also observed that PDA does not pose any cytotoxicity risk to cells *in vitro*, thus supporting their further use in *in vivo* studies. Our *in vivo* experiments got the expected results and revealed that a PDA coating significantly increased the retention of fluorescent beads

sprayed onto the mouse heart as compared to those without the PDA coating. These results support our future studies, wherein PDA will be used to coat on nanoparticles carrying therapeutic agents that will be delivered at the myocardial infarct site. The results expected at the end of the next part of this research will be better therapeutic effects at the infarct site due to increased retention of PDA-coated nanoparticles. Based on the results carried out in my thesis, PDA-coated nanoparticles should adhere at the infarct site in greater numbers and for a longer period of time and this will allow them to release the therapeutic agents more effectively as compared to that of non-coated nanoparticles. Ultimately, functionalized nanoparticles are a promising approach to improve the reparative effects of their therapeutic cargo, thus improving heart function post-MI.

Bibliography

[1] D. Mozaffarian *et al.*, “Heart Disease and Stroke Statistics—2015 Update,” *Circulation*, vol. 131, no. 4, pp. e29–e39, Jan. 2015.

[2] M. M. Nguyen *et al.*, “Enzyme-Responsive Nanoparticles for Targeted Accumulation and Prolonged Retention in Heart Tissue after Myocardial Infarction,” *Adv. Mater.*, vol. 27, no. 37, pp. 5547–5552, Oct. 2015.

[3] G. A. Roth *et al.*, “Global, regional, and national age-sex-specific mortality for 282 causes of death in 195 countries and territories, 1980-2017: a systematic analysis for the Global Burden of Disease Study 2017,” *Lancet (London, England)*, vol. 392, no. 10159, pp. 1736–1788, Nov. 2018.

[4] J. A. Reyes-Retana and L. C. Duque-Ossa, “Acute Myocardial Infarction Biosensor: A Review From Bottom Up,” *Curr. Probl. Cardiol.*, vol. 46, no. 3, p. 100739, Mar. 2021.

[5] M. Saleh and J. A. Ambrose, “Understanding myocardial infarction,” *F1000Research*, vol. 7, 2018.

[6] H. D. White and D. P. Chew, “Acute myocardial infarction,” *Lancet*, vol. 372, no. 9638, pp. 570–584, Aug. 2008.

[7] K. Thygesen, J. S. Alpert, and H. D. White, “Universal Definition of Myocardial Infarction,” *J. Am. Coll. Cardiol.*, vol. 50, no. 22, pp. 2173–2195, Nov. 2007.

[8] N. G. Frangogiannis, “Pathophysiology of Myocardial Infarction,” *Compr. Physiol.*, vol. 5, no. 4, pp. 1841–1875, Oct. 2015.

[9] S. Hashmi and S. Al-Salam, “Acute myocardial infarction and myocardial ischemia-reperfusion injury: a comparison,” *Int. J. Clin. Exp. Pathol.*, vol. 8, no. 8, p. 8786, 2015.

[10] R. A. Gottlieb, K. O. Burleson, R. A. Kloner, B. M. Babior, and R. L. Engler, “Reperfusion injury induces apoptosis in rabbit cardiomyocytes,” *J. Clin. Invest.*, vol. 94, no. 4, pp. 1621–1628, 1994.

[11] W. Cheng *et al.*, “Stretch-induced programmed myocyte cell death,” *J. Clin. Invest.*, vol. 96, no. 5, pp. 2247–2259, 1995.

[12] P. Anversa, W. Cheng, Y. Liu, A. Leri, G. Redaelli, and J. Kajstura, "Apoptosis and myocardial infarction," *Basic Res. Cardiol. 1998 933*, vol. 93, no. 3, pp. s008-s012, Sep. 1998.

[13] "Apoptotic and necrotic myocyte cell deaths are independent contributing variables of infarct size in rats - PubMed." [Online]. Available: https://pubmed.ncbi.nlm.nih.gov/8569201/. [Accessed: 30-May-2022].

[14] W. Cheng *et al.*, "Programmed myocyte cell death affects the viable myocardium after infarction in rats," *Exp. Cell Res.*, vol. 226, no. 2, pp. 316–327, Aug. 1996.

[15] Z. Lister, K. J. Rayner, and E. J. Suuronen, "How biomaterials can influence various cell types in the repair and regeneration of the heart after myocardial infarction," *Front. Bioeng. Biotechnol.*, vol. 4, no. JUL, p. 62, Jul. 2016.

[16] M. Nahrendorf, M. J. Pittet, and F. K. Swirski, "Monocytes: Protagonists of infarct inflammation and repair after myocardial infarction," *Circulation*, vol. 121, no. 22, pp. 2437–2445, Jun. 2010.

[17] H. Wang *et al.*, "Promotion of cardiac differentiation of brown adipose derived stem cells by chitosan hydrogel for repair after myocardial infarction," *Biomaterials*, vol. 35, no. 13, pp. 3986–3998, Apr. 2014.

[18] D. Fraccarollo and J. Bauersachs, "Cardiomyocyte Mineralocorticoid Receptor Function Post Myocardial Infarction," *Trends Cardiovasc. Med.*, vol. 21, no. 2, pp. 42–47, Feb. 2011.

[19] G. Ertl and S. Frantz, "Healing after myocardial infarction," *Cardiovasc. Res.*, vol. 66, no. 1, pp. 22–32, Apr. 2005.

[20] H. Takahama *et al.*, "Prolonged Targeting of Ischemic/Reperfused Myocardium by Liposomal Adenosine Augments Cardioprotection in Rats," *J. Am. Coll. Cardiol.*, vol. 53, no. 8, pp. 709–717, Feb. 2009.

[21] A. A. Rane and K. L. Christman, "Biomaterials for the treatment of myocardial infarction: a 5-year update," *J. Am. Coll. Cardiol.*, vol. 58, no. 25, pp. 2615–2629, Dec. 2011.

[22] W. J. M. Mulder, A. W. Griffioen, G. J. Strijkers, D. P. Cormode, K. Nicolay, and Z. A. Fayad, "Magnetic and fluorescent nanoparticles for multimodality imaging," *https://doi.org/10.2217/17435889.2.3.307*, vol. 2, no. 3, pp. 307–324, Jun. 2007.

[23] J. S. Golub *et al.*, "Sustained VEGF delivery via PLGA nanoparticles promotes vascular growth," *Am. J. Physiol. Heart Circ. Physiol.*, vol. 298, no. 6, Jun. 2010.

[24] P. Díaz-Herráez *et al.*, "Transplantation of adipose-derived stem cells combined with neuregulin-microparticles promotes efficient cardiac repair in a rat myocardial infarction model," *J. Control. Release*, vol. 249, pp. 23–31, Mar. 2017.

[25] Y. Nakano *et al.*, "Nanoparticle-Mediated Delivery of Irbesartan Induces Cardioprotection from Myocardial Ischemia-Reperfusion Injury by Antagonizing Monocyte-Mediated Inflammation," *Sci. Reports 2016 61*, vol. 6, no. 1, pp. 1–14,

Jul. 2016.

[26] L. Han *et al.*, "Tough, self-healable and tissue-adhesive hydrogel with tunable multifunctionality," *NPG Asia Mater.*, vol. 9, no. 4, 2017.

[27] H. G. Silverman and F. F. Roberto, "Understanding marine mussel adhesion," *Mar. Biotechnol. (NY).*, vol. 9, no. 6, pp. 661–681, Dec. 2007.

[28] J. H. Waite and X. Qin, "Polyphosphoprotein from the adhesive pads of Mytilus edulis," *Biochemistry*, vol. 40, no. 9, pp. 2887–2893, Mar. 2001.

[29] J. H. Ryu, P. B. Messersmith, and H. Lee, "Polydopamine Surface Chemistry: A Decade of Discovery," *ACS Appl. Mater. Interfaces*, vol. 10, no. 9, p. 7523, Mar. 2018.

[30] M. V. Rapp *et al.*, "Defining the Catechol-Cation Synergy for Enhanced Wet Adhesion to Mineral Surfaces," *J. Am. Chem. Soc.*, vol. 138, no. 29, pp. 9013–9016, Jul. 2016.

[31] S.-C. Chou, W.-A. Chung, T.-L. Fan, Y. Dordi, J. Koike, and P.-W. Wu, "Polydopamine and Its Composite Film as an Adhesion Layer for Cu Electroless Deposition on SiO2," *J. Electrochem. Soc.*, vol. 167, no. 4, p. 042507, Mar. 2020.

[32] N. T. Tran, D. P. Flanagan, J. A. Orlicki, J. L. Lenhart, K. L. Proctor, and D. B. Knorr, "Polydopamine and Polydopamine-Silane Hybrid Surface Treatments in Structural Adhesive Applications," *Langmuir*, vol. 34, no. 4, pp. 1274–1286, Jan. 2018.

[33] J. Saiz-Poseu, J. Mancebo-Aracil, F. Nador, F. Busqué, and D. Ruiz-Molina, "The Chemistry behind Catechol-Based Adhesion," *Angew. Chemie - Int. Ed.*, vol. 58, no. 3, pp. 696–714, 2019.

[34] P. Kord Forooshani and B. P. Lee, "Recent approaches in designing bioadhesive materials inspired by mussel adhesive protein," *J. Polym. Sci. A. Polym. Chem.*, vol. 55, no. 1, pp. 9–33, Jan. 2017.

[35] M. Liang *et al.*, "A high-strength double network polydopamine nanocomposite hydrogel for adhesion under seawater," *J. Mater. Chem. B*, vol. 8, no. 36, pp. 8232–8241, Sep. 2020.

[36] C. C. Ho and S. J. Ding, "The pH-controlled nanoparticles size of polydopamine for anti-cancer drug delivery," *J. Mater. Sci. Mater. Med. 2013 2410*, vol. 24, no. 10, pp. 2381–2390, Jun. 2013.

[37] V. Ball, "Polydopamine nanomaterials: Recent advances in synthesis methods and applications," *Front. Bioeng. Biotechnol.*, vol. 6, no. AUG, p. 109, Aug. 2018.

[38] Q. Wei, F. Zhang, J. Li, B. Li, and C. Zhao, "Oxidant -induced dopamine polymerization for multifunctional coatings," *Polym. Chem.*, vol. 1, no. 9, pp. 1430–1433, Oct. 2010.

[39] X. Du *et al.*, "UV-Triggered Dopamine Polymerization: Control of

Polymerization, Surface Coating, and Photopatterning," *Adv. Mater.*, vol. 26, no. 47, pp. 8029–8033, Dec. 2014.

[40] Y. Li, M. Liu, C. Xiang, Q. Xie, and S. Yao, "Electrochemical quartz crystal microbalance study on growth and property of the polymer deposit at gold electrodes during oxidation of dopamine in aqueous solutions," *Thin Solid Films*, vol. 497, no. 1–2, pp. 270–278, Feb. 2006.

[41] V. Ball *et al.*, "Deposition Mechanism and Properties of Thin Polydopamine Films for High Added Value Applications in Surface Science at the Nanoscale," *BioNanoScience 2011 21*, vol. 2, no. 1, pp. 16–34, Dec. 2011.

[42] C. Schlaich *et al.*, "Mussel-Inspired Polymer-Based Universal Spray Coating for Surface Modification: Fast Fabrication of Antibacterial and Superhydrophobic Surface Coatings," *Adv. Mater. Interfaces*, vol. 5, no. 5, p. 1701254, Mar. 2018.

[43] F. Ponzio *et al.*, "Robust Alginate-Catechol@Polydopamine Free-Standing Membranes Obtained from the Water/Air Interface," *Langmuir*, vol. 33, no. 9, pp. 2420–2426, Mar. 2017.

[44] N. Orishchin *et al.*, "Rapid Deposition of Uniform Polydopamine Coatings on Nanoparticle Surfaces with Controllable Thickness," *Langmuir*, vol. 33, no. 24, pp. 6046–6053, Jun. 2017.

[45] P. Zhou *et al.*, "Rapidly-Deposited Polydopamine Coating via High Temperature and Vigorous Stirring: Formation, Characterization and Biofunctional Evaluation," *PLoS One*, vol. 9, no. 11, p. e113087, Nov. 2014.

[46] K. Kang, I. S. Choi, and Y. Nam, "A biofunctionalization scheme for neural interfaces using polydopamine polymer," *Biomaterials*, vol. 32, no. 27, pp. 6374–6380, Sep. 2011.

[47] Y. Bin Lee *et al.*, "Polydopamine-mediated immobilization of multiple bioactive molecules for the development of functional vascular graft materials," *Biomaterials*, vol. 33, no. 33, pp. 8343–8352, Nov. 2012.

[48] E. Meyer, "Atomic force microscopy," *Prog. Surf. Sci.*, vol. 41, no. 1, pp. 3–49, Sep. 1992.

[49] "Atomic Force Microscopy (AFM) - WITec Raman Imaging - Oxford Instruments." [Online]. Available: https://raman.oxinst.com/techniques/scanning-probe-microscopy. [Accessed: 17-Aug-2022].

[50] D. Rugar and P. Hansma, "Atomic force microscopy," *Phys. Today*, vol. 43, no. 10, pp. 23–30, 1990.

[51] R. García and R. Pérez, "Dynamic atomic force microscopy methods," *Surf. Sci. Rep.*, vol. 47, no. 6–8, pp. 197–301, Sep. 2002.

[52] M. Meincken, S. P. Roux, and E. P. Jacobs, "Determination of the hydrophilic character of membranes by pulsed force mode atomic force microscopy," *Appl. Surf. Sci.*, vol. 252, no. 5, pp. 1772–1779, Dec. 2005.

[53] H. J. Butt, B. Cappella, and M. Kappl, “Force measurements with the atomic force microscope: Technique, interpretation and applications,” *Surf. Sci. Rep.*, vol. 59, no. 1–6, pp. 1–152, Oct. 2005.

[54] B. Cappella and G. Dietler, “Force-distance curves by atomic force microscopy,” *Surf. Sci. Rep.*, vol. 34, no. 1–3, pp. 1–104, Jan. 1999.

[55] R. J. Cannara, M. Eglin, and R. W. Carpick, “Lateral force calibration in atomic force microscopy: A new lateral force calibration method and general guidelines for optimization,” *Rev. Sci. Instrum.*, vol. 77, no. 5, p. 053701, May 2006.

[56] J. Rao, A. Dragulescu-Andrasi, and H. Yao, “Fluorescence imaging in vivo: recent advances,” *Curr. Opin. Biotechnol.*, vol. 18, no. 1, pp. 17–25, Feb. 2007.

[57] “In Vivo Imaging Systems - Berthold Technologies GmbH & Co.KG.” [Online]. Available: https://www.berthold.com/en-us/bioanalytic/products/in-vivo-imaging-systems/. [Accessed: 19-Aug-2022].

[58] R. Weissleder, “A clearer vision for in vivo imaging,” *Nat. Biotechnol. 2001 194*, vol. 19, no. 4, pp. 316–317, 2001.

[59] P. Inc, “IVIS Spectrum Pre-Clinical Optical Imaging System.”

[60] N. Blow, “In vivo molecular imaging: the inside job,” *Nat. Methods 2009 66*, vol. 6, no. 6, pp. 465–469, 2009.

[61] S. Andersson-Engels, C. A. Klinteberg, K. Svanberg, and S. Svanberg, “In vivo fluorescence imaging for tissue diagnostics,” *Phys. Med. Biol.*, vol. 42, no. 5, p. 815, May 1997.

[62] N. Deshpande, Y. Ren, K. Foygel, J. Rosenberg, and J. K. Willmann, “Non-invasive in vivo imaging in small animal research,” *Anal. Cell. Pathol.*, vol. 28, no. 4, pp. 127–139, Jan. 2006.

[63] Y. Ding *et al.*, “Insights into the Aggregation/Deposition and Structure of a Polydopamine Film,” *Langmuir*, vol. 30, no. 41, pp. 12258–12269, Oct. 2014.

[64] “(PDF) A Technique for Direct Measurement of UV Fluence Distribution.” [Online]. Available: https://www.researchgate.net/publication/304608192_A_Technique_for_Direct_Measurement_of_UV_Fluence_Distribution#pf7. [Accessed: 24-Feb-2022].

[65] M. Muñoz *et al.*, “Nanoengineered Sprayable Therapy for Treating Myocardial Infarction,” *ACS Nano*, vol. 16, no. 3, pp. 3522–3537, Mar. 2022.

[66] Q. Liu, B. Yu, W. Ye, and F. Zhou, “Highly selective uptake and release of charged molecules by pH-responsive polydopamine microcapsules,” *Macromol. Biosci.*, vol. 11, no. 9, pp. 1227–1234, Sep. 2011.

[67] J. Liebscher, “Chemistry of Polydopamine – Scope, Variation, and Limitation,” *European J. Org. Chem.*, vol. 2019, no. 31–32, pp. 4976–4994, Sep. 2019.

[68] B. Yu, J. Liu, S. Liu, and F. Zhou, “Pdop layer exhibiting zwitterionicity: A simple electrochemical interface for governing ion permeability,” *Chem. Commun.*, vol. 46, no. 32, pp. 5900–5902, Aug. 2010.

[69] H. Lee, S. M. Dellatore, W. M. Miller, and P. B. Messersmith, “Mussel-inspired surface chemistry for multifunctional coatings,” *Science (80-.).*, vol. 318, no. 5849, pp. 426–430, Oct. 2007.

[70] K. M. Im, T. W. Kim, and J. R. Jeon, “Metal-Chelation-Assisted Deposition of Polydopamine on Human Hair: A Ready-to-Use Eumelanin-Based Hair Dyeing Methodology,” *ACS Biomater. Sci. Eng.*, vol. 3, no. 4, pp. 628–636, Apr. 2017.

[71] A. Schneider *et al.*, “Boric Acid as an Efficient Agent for the Control of Polydopamine Self-Assembly and Surface Properties,” *ACS Appl. Mater. Interfaces*, vol. 10, no. 9, pp. 7574–7580, Mar. 2018.

[72] P. Zhang *et al.*, “Cost-Effective Strategy for Surface Modification via Complexation of Disassembled Polydopamine with Fe(III) Ions,” *Langmuir*, vol. 35, no. 11, pp. 4101–4109, Mar. 2019.

[73] H. Li, D. Yin, W. Li, Q. Tang, L. Zou, and Q. Peng, “Polydopamine-based nanomaterials and their potentials in advanced drug delivery and therapy,” *Colloids Surf. B. Biointerfaces*, vol. 199, Mar. 2021.

[74] L. Han *et al.*, “Polydopamine/polystyrene nanocomposite double-layer strain sensor hydrogel with mechanical, self-healing, adhesive and conductive properties,” *Mater. Sci. Eng. C*, vol. 109, p. 110567, Apr. 2020.

[75] N. Orishchin *et al.*, “Rapid Deposition of Uniform Polydopamine Coatings on Nanoparticle Surfaces with Controllable Thickness,” *Langmuir*, vol. 33, no. 24, pp. 6046–6053, Jun. 2017.

[76] X. Liu *et al.*, “Mussel-inspired polydopamine: A biocompatible and ultrastable coating for nanoparticles in vivo,” *ACS Nano*, vol. 7, no. 10, pp. 9384–9395, Oct. 2013.

[77] S. Hong *et al.*, “Attenuation of the in vivo toxicity of biomaterials by polydopamine surface modification,” *Nanomedicine*, vol. 6, no. 5, pp. 793–801, Jul. 2011.

[78] S. Hong *et al.*, “Attenuation of the in vivo toxicity of biomaterials by polydopamine surface modification,” *Nanomedicine (Lond).*, vol. 6, no. 5, pp. 793–801, Jul. 2011.

[79] S. H. Ku and C. B. Park, “Human endothelial cell growth on mussel-inspired nanofiber scaffold for vascular tissue engineering,” *Biomaterials*, vol. 31, no. 36, pp. 9431–9437, Dec. 2010.

Appendix

Copyright and Permissions

WOLTERS KLUWER HEALTH, INC. LICENSE
TERMS AND CONDITIONS

Feb 09, 2023

This Agreement between Ms. Roja Gauda ("You") and Wolters Kluwer Health, Inc. ("Wolters Kluwer Health, Inc.") consists of your license details and the terms and conditions provided by Wolters Kluwer Health, Inc. and Copyright Clearance Center.

License Number	5483701246940
License date	Feb 07, 2023
Licensed Content Publisher	Wolters Kluwer Health, Inc.
Licensed Content Publication	Circulation
Licensed Content Title	Monocytes: Protagonists of Infarct Inflammation and Repair After Myocardial Infarction
Licensed Content Author	Matthias Nahrendorf, Mikael J. Pittet, Filip K. Swirski
Licensed Content Date	Jun 8, 2010
Licensed Content Volume	121
Licensed Content Issue	22
Type of Use	Dissertation/Thesis
Requestor type	University/College
Sponsorship	No Sponsorship
Format	Electronic

JOHN WILEY AND SONS LICENSE
TERMS AND CONDITIONS

Feb 07, 2023

This Agreement between Ms. Roja Gauda ("You") and John Wiley and Sons ("John Wiley and Sons") consists of your license details and the terms and conditions provided by John Wiley and Sons and Copyright Clearance Center.

License Number	5480640636113
License date	Feb 02, 2023
Licensed Content Publisher	John Wiley and Sons
Licensed Content Publication	Angewandte Chemie International Edition
Licensed Content Title	The Chemistry behind Catechol-Based Adhesion
Licensed Content Author	D. Ruiz-Molina, F. Busqué, F. Nador, et al
Licensed Content Date	Oct 25, 2018
Licensed Content Volume	58
Licensed Content Issue	3
Licensed Content Pages	19
Type of use	Dissertation/Thesis
Requestor type	University/Academic